

# Synthesis and characterization of Pd(II) antitumor complex, DFT calculation and DNA/BSA binding insight through the combined experimental and theoretical aspects

Mehran Feizi-Dehghanian, Effat Dehghanian\*, Hassan Mansouri-Torshizi

Department of Chemistry, University of Sistan and Baluchestan, Zahedan, Iran

## ARTICLE INFO

### Article history:

Received 16 January 2021

Revised 12 April 2021

Accepted 19 April 2021

Available online 24 April 2021

### Keywords:

K562

DFT calculation

FMO

Biomolecules

Molecular docking

## ABSTRACT

A novel palladium(II) complex,  $[\text{Pd}(\text{bpy})(\text{acac})]\text{NO}_3$  (where bpy and acac are 2,2'-bipyridine and acetylacetonato), has been synthesized and fully characterized through  $^1\text{H}$  NMR, UV-Vis and FT-IR spectra, conductivity measurement and elemental analysis. Geometry optimization using DFT calculation demonstrated that a square-planar geometry is built around Pd(II) atom. The MEP and FMO analysis were also applied. Partition coefficient evaluation was conducted to determine the lipophilicity of the compound which follows the order complex > cisplatin. The antitumor activity of the complex has been evaluated on K562 cancer cells by MTT method, which exhibited an appropriate activity in compare to cisplatin. The interaction of  $[\text{Pd}(\text{bpy})(\text{acac})]\text{NO}_3$  towards biomolecules (CT-DNA and BSA) was investigated through in-detail fluorescence, UV-Vis and other techniques. The findings of fluorescence titration demonstrated that the Pd(II) complex binds to CT-DNA via hydrophobic and with BSA through van der Waals forces and hydrogen bond. UV-Vis experiment revealed a reduction in the absorption spectra of biomolecules in presence of the complex. The binding affinity was further endorsed for CT-DNA utilizing viscosity measurement and gel electrophoresis and for BSA via CD spectroscopy and FRET calculation. In addition, molecular docking supports the findings of experiments and indicates that the Pd(II) complex appears to be situated at DNA intercalation position and BSA Sudlow's site I. All results have shown that this compound may be a useful potential antitumor candidate for further medical purposes.

© 2021 Elsevier B.V. All rights reserved.

## 1. Introduction

Cisplatin is a chemotropic drug discovered by Rosenberg [1] and currently administered in several types of cancers such as colorectal, testicular, ovarian, and lymphoma [2,3]. One accepted hypothesis about the mechanism of action for cisplatin ( $\text{cis-}[\text{PtCl}_2(\text{NH}_3)_2]$ ) as an anticancer compound is that when it enters a cell, hydrolysis happens and two chloride ligands are replaced by water molecules. As a result, the ionic complex with positive charge is produced which has a tendency to interact with nucleophilic species like DNA. This action distorts DNA and causes cytotoxicity property of platinum based complexes including cisplatin. Since amine groups ( $\text{NH}_3$ ) are the same in cisplatin, carboplatin, and nedaplatin (Fig. 1), therefore they may demonstrate equivalent DNA binding mode. On the other hand, platinum based complexes have drastic potency for interacting with sulfur in the amino acids

of proteins and peptides. This leads to inactivation of platinum complexes, severe side effects, and cellular resistance [4]. These drawbacks of platinum based complexes are a motivation for synthesis and testing new anticancer agents with different transition metals.

Since both platinum(II) and palladium(II) ions have  $d^8$  electron configuration and nearly the same size, so they exhibit similar chemical properties and form square planar complexes [5]. As a result, therapeutics effects and antitumor activity of palladium is of interest for further studies. However, Pd-complexes are more labile and reactive than Pt-analogs where by choosing appropriate chelate ligand, one can keep this reactivity at the reasonable limit and in accordance with biological system conditions. Some researchers have demonstrated that many palladium complexes show anticancer activity at  $\text{pH} = 6.8$  that belongs to cancer cell lines where healthy cells live in  $\text{pH} = 7.4$  [6]. Another interesting point about palladium complexes is that some of trans complexes have more cytotoxicity activity than cis ones [7].

2,2'-bipyridine ligand (bpy) consists of two aromatic nitrogen-containing pyridine ( $\text{C}_5\text{H}_4\text{N}$ ) rings. Such a pyridine ring interacts with metals mostly as a  $\sigma$ -donor/ $\pi$ -acceptor agent. Since the dis-

\* Corresponding author.

E-mail addresses: [m.feizi@sutec.ac.ir](mailto:m.feizi@sutec.ac.ir) (M. Feizi-Dehghanian), [dehghanian@chem.usb.ac.ir](mailto:dehghanian@chem.usb.ac.ir) (E. Dehghanian), [hmtorshizi@hamoon.usb.ac.ir](mailto:hmtorshizi@hamoon.usb.ac.ir) (H. Mansouri-Torshizi).

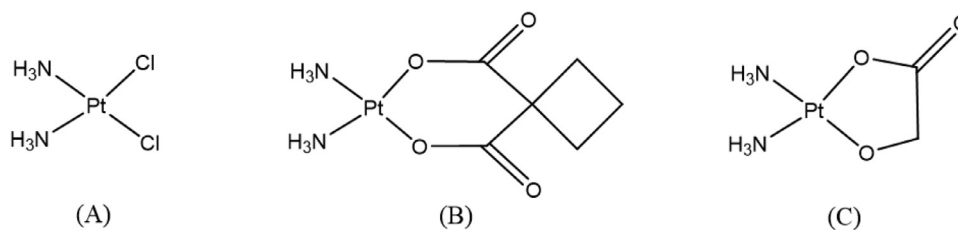


Fig. 1. Molecular structure of platinum based complexes with two  $\text{NH}_3$  ligands (A: cisplatin, B: carboplatin, and C: nedaplatin).

covery of bpy at the end of nineteenth century [8] it has been largely used in the synthesis of complexes with metal ions. As it is a neutral compound it forms charged complexes with transition metal ions. Acetylacetone, an organic molecule with the general formula  $\text{CH}_3\text{COCH}_2\text{COCH}_3$ , is commonly abbreviated to acac, is an appropriate chelating compound as i) it is available at proper cost ii) it forms stable chelating complexes with over 60 metals even at low concentration of metals and iii) it is soluble in organic as well as some inorganic solvents [9].

DNA or deoxyribonucleic acid [10] is the hereditary substance that carries genetic information in almost all organisms. Each DNA includes a backbone of sugar and phosphate along with some attached bases to it. The name is taken from its combination, in the other word, "deoxyribo" refers to the sugar and the nucleic acid refers to the bases and phosphate. The bases are adenine, cytosine, guanine, and thymine, where their pattern encodes huge complexity. DNA is assumed to be the main target for anticancer drugs, because it is involved in important mechanisms in the cells. So, the definitive target for palladium based complexes is widely accepted to be DNA. But the exact mechanism by which the palladium based compounds interact with DNA and lead to the cell death is unknown.

Serum albumin (SA) is the most abundant protein in the bloodstream of many organisms and some tissues. Investigating the interaction between albumin and drug is essential and of vital importance since the distribution and action of many drugs are related with their binding affinities to SA. Bovine serum albumin (BSA) is often chosen as protein model for human serum albumin (HSA) because of structural similarity to HSA, unusual binding properties, water solubility, availability and its low cost [11]. It is composed of 3 homologous domains i.e., I, II, and III and 2 subdomains (A and B). BSA has 2 tryptophan residues (Trp134 and Trp212) that have intrinsic fluorescence emission property [12].

Keeping the above subject matters in mind, we intend to synthesize and characterize the new water-soluble palladium(II) complex. Partition coefficient value of the complex was determined to check the lipophilicity of the palladium(II) complex in comparison to cisplatin. The antitumor activity of the complex was determined for cancer cells by MTT assay. Density functional theory (DFT) calculations i.e. geometry optimization, frontier molecular orbital (FMO) analysis and molecular electrostatic potential (MEP) surface were conducted in the gas phase. The in-detail interaction of  $[\text{Pd}(\text{bpy})(\text{acac})]\text{NO}_3$  with DNA as the principal target of anticancer agents and BSA as a transport protein in the blood circulation was investigated by different experimental methods. In addition, in order to predict the correlation between computational and experimental results, the compound has been interacted with DNA and BSA via *in-silico* molecular modeling.

## 2. Experimental

### 2.1. Material and method

Acetyl acetone, NaCl, ethidium bromide (EB),  $\text{PdCl}_2$ , NaOH,  $\text{AgNO}_3$  and 2,2'-bipyridine were bought from Merck chemical

company. CT-DNA (Calf thymus DNA, highly polymerized-type1), Tris-HCl buffer and BSA were obtained from Sigma-Aldrich and commercial solvents (Merck) including acetonitrile, ethanol, acetone and methanol were reagent grade and were used as received. Deionized water was utilized all over measurements. Similar synthetic procedure [13] was carried out for the preparation of  $[\text{Pd}(\text{bpy})\text{Cl}_2]$ .

Fourier Transfer Infrared (FT-IR) spectra of the complex and ligands were measured in KBr pellets on a Perkin Elmer FT-IR spectrometer ( $400\text{--}4000\text{ cm}^{-1}$ ). UV-Vis spectra of free metal complex and interacted metal complex with biomolecules were taken utilizing a JASCO, V-570. The lipophilicity value of the compound was evaluated utilizing partition coefficient experiment by shake-flask method. Molar conductivity of the Pd(II) complex was measured on HANA-EC215, using deionized water.  $^1\text{H}$  NMR spectrum of the synthesized metal complex was recorded in the range of 0–12 ppm by a Bruker-250 NMR spectrometer utilizing DMSO- $d_6$  as solvent and TMS as standard reference. Elemental analysis for CHN was conducted on a Heraeus CHNO-RAPID elemental analyzer. Using the fluorescence spectrometer, Cary Eclipse, the emission patterns of the samples were measured. The circular dichroism (CD) measurement of BSA in the presence and absence of Pd(II) complex were recorded through Aviv-215 CD spectrometer, USA. Using Maxi HD  $15 \times 15$  Tank, Ladder 100 bp, electrophoresis assay was performed on CCD-5 Gel Doc System. Decomposition temperature of complex was measured through electrothermal model 9100 using glass capillary and are uncorrected. Viscosity experiments were performed utilizing Ostwald micro-viscometer (SCHOT-geräte) at ambient temperature of  $27 \pm 1\text{ }^\circ\text{C}$ .

### 2.2. Synthesis process of $[\text{Pd}(\text{bpy})(\text{acac})]\text{NO}_3$

Acetylacetonato-2,2'-bipyridinepalladium(II) nitrate,  $\text{C}_{15}\text{H}_{15}\text{N}_3\text{O}_5$   
Pd = 423 g/mol

0.1 mL (1 mmol) of acetyl acetone and 0.04 g (1 mmol) of NaOH were dissolved in a blend of water and ethanol (20 mL, 1:1 V/V) and stirred at  $40\text{ }^\circ\text{C}$  for 20 min for obtaining sodium salt of acetyl acetate. This mixture was poured on a suspension of  $[\text{Pd}(\text{bpy})\text{Cl}_2]$  (0.333 g, 1 mmol) in 50 mL double distilled water and stirred for 2 h at  $50\text{ }^\circ\text{C}$ . It was then cooled to  $28\text{ }^\circ\text{C}$  and 2 mmol (0.335 g) of  $\text{AgNO}_3$  in 10 mL water was added and stirred at  $50\text{ }^\circ\text{C}$  for 7 h in dark. Stirring continued at room temperature for another 12 h. The AgCl precipitate was filtered off through Wattman 42 filter paper. The volume of yellowish filtrate was reduced by evaporation at  $45\text{ }^\circ\text{C}$  to 35 mL and filtered again. Evaporation was continued to 7 mL and left a side overnight. The obtained yellow precipitate was filtered, washed with acetone and dried in an oven at  $50\text{ }^\circ\text{C}$ . Recrystallization was carried out via dissolving the precipitate in a 5 mL mixture of acetonitrile methanol (1:1 V/V). On diffusing diethyl ether to this blend for 72 h, the cauliflower shaped precipitate was formed which was filtered, washed with acetone and dried in an oven at  $50\text{ }^\circ\text{C}$ . Yield: 0.44 g (70%) and decomposed at  $226\text{--}228\text{ }^\circ\text{C}$ . The suggested equations are illustrated in Fig. 2.

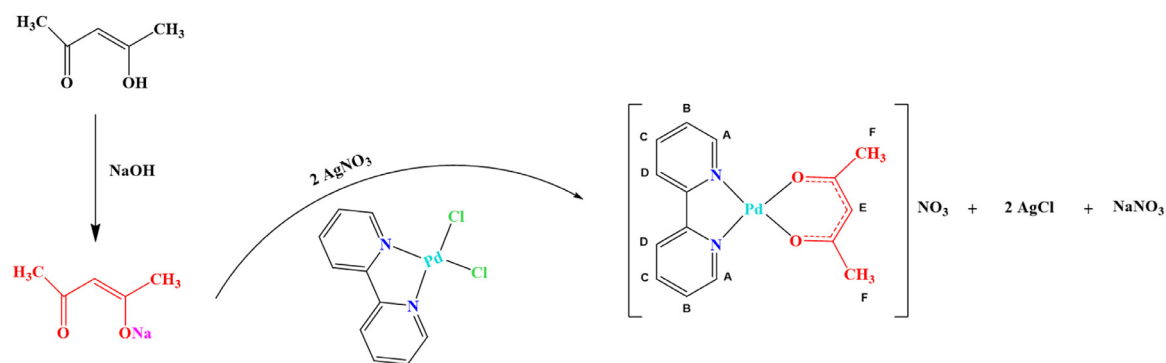


Fig. 2. Structure and reactions suggested for  $[Pd(bpy)(acac)]NO_3$  complex involving  $^1H$  NMR signing scheme.

### 2.3. Computational details

The initial 3D structure of Pd(II) complex and its related ligands were built using Gauss view 5.0 software. DFT method has been applied to achieve an insight into the palladium(II) complex and ligands electronic structure in the gas phase through Gaussian 09 software. The B3LYP (the Becke's exchange functional [14] and the Lee, Yang and Parr's [15] correlation functional)/GENECP (with effective core pseudo potentials) level of theory were applied for geometry optimization and frequency calculations of ground state [16]. Aug-cc-pVTZ-PP, and 6-311 g(d) basis sets were used for Pd and nonmetal atoms (H, C, N and O), respectively [17-19]. The calculated structure was confirmed to be at true minimum (lack of imaginary vibrational frequencies) on global PES (potential energy surface). Also, molecular orbital studies (electronic properties and global reactivity parameters) and MEP analysis were carried out by using Gauss View 5.0 software package.

### 2.4. Stability test

In general, electronic absorption spectrum of a given compound is recorded in order to determine its stability in aqueous media. A solution of  $[Pd(bpy)(acac)]NO_3$  (0.001 g/10 mL) in double distilled water or Tris-HCl buffer was prepared and stirred in a thermostatic water bath of 37 °C. Then, the electronic absorption spectrum of this sample was measured from 0 to 20 h to check if there is disappearance or any change in the peak position with the time.

### 2.5. Partition coefficients determination

The lipophilicity value of the Pd (II) complex was determined utilizing "shake flask" method in a blend of deionized water and n-octanol media [20]. At first,  $[Pd(bpy)(acac)]NO_3$  (0.001 g) was dissolved in a blend of water-octanol (10 mL, 1:1v/v) via shaking for 12 h. Then, this blend was left a side at ambient temperature for one h to achieve phase separation. The concentration of the Pd(II) complex in each layer (octanol and water) was determined from their UV-Vis spectra. Finally, the lipophilicity value of the complex was obtained in terms of partition coefficient (log P) via the following formula:

$$\log P = \log \left( \frac{[Pd(II) \text{ complex}]_{in \text{ octanol}}}{[Pd(II) \text{ complex}]_{in \text{ water}}} \right) \quad (1)$$

### 2.6. In-vitro cytotoxicity experiment

The leukemia cell line, K562, was received from Pasteur Institute cell bank (Iran), which was kept in RPMI (Roswell Park Memorial Institute, 1640-medium) filled with fetal calf serum (FCS, 10%), 5  $\mu$ g/mL penicillin and  $2 \times 10^{-3}$  M L-glutamine at 37 °C.

The cells were cultivated in humidified conditions (5% CO<sub>2</sub> and 95% air atmosphere). The MTT (3-(4,5-dimethylthiazol-yl)-2,5-diphenyltetrazolium bromide) assay was applied for the measurement of cytotoxicity effect of this complex against the cells [21]. This experiment is dependent on the conversion and cleavage of MTT to formazan via active mitochondrial dehydrogenase of living cells. Harvested sample cells were seeded into a 96-well culture plate ( $1.5 \times 10^4$  cell/mL) with diverse concentrations of the  $[Pd(bpy)(acac)]NO_3$  from 0 to 100  $\mu$ M and incubated for 24 h. Before the end of incubations step, 25  $\mu$ L of MTT solution (5 mg/mL) in PBS was poured into each well-plate. The resulted formazan precipitates were dissolved in a 50% DMF solution and sodium dodecyl sulfate (SDS, 10%) and incubated for 3 h at 37 °C in dark. Optical density (OD) was read to reagent blank utilizing ELISA Reader-Model Expert 96 (Austria) at 570 nm. In this assay, absorbance is a function of converted dye concentration. The viability of each study group was reported as percentage control absorbance and specified as 50% inhibition concentration (IC<sub>50</sub>) [22].

### 2.7. Macromolecules-metal complex binding studies

All solutions in this work were freshly prepared before any usage. BSA (3 mg/mL) and CT-DNA (1.5 mg/mL) stock solutions were prepared in Tris-HCl buffer, pH = 7.2, and stirred at 4 °C till homogenous and kept for no more than 10 days. Concentrated stock solution of the complex was dissolved in deionized water to get the concentration of  $10^{-4}$  M for biomolecules binding studies. The concentration of biomolecules was obtained spectrophotometrically utilizing the values of molar extinction coefficients ( $\epsilon$  DNA, 260 nm =  $6600 \text{ M}^{-1}\text{cm}^{-1}$  and  $\epsilon$  BSA, 280 nm =  $44,300 \text{ M}^{-1}\text{cm}^{-1}$ ) [23,24]. The binding affinities between the metal complex and biomolecules were described through variety of following methods.

#### 2.7.1. UV-Vis experiments

Two titration measurements were performed using UV-Vis spectroscopy in the range of 200–700 nm at 300 K. In the first measurement, 1.97 and 1.55 mL of Tris-HCl buffer was added separately to 30  $\mu$ L of CT-DNA stock solution and 450  $\mu$ L of BSA stock solution to attain the overall volume of 2 mL and were mixed until homogenized. The resulted solutions were titrated via metal complex stock solution (20 to 300  $\mu$ L for DNA and 250 to 1250  $\mu$ L for BSA). After each step of addition, the resulting solution was remained for 3 min to equilibrate, then the UV pattern was measured. In both measurements, an equivalent volume of Pd(II) complex was added to the reference cell in order to delete the compound absorbance at 260 and 280 nm for CT-DNA and BSA solution, respectively. From the absorption data, we can evaluate the apparent binding constant ( $K_{app}$ ) for the biomolecule-metal com-

plex according to the Eq. (2) [25,26]:

$$\frac{1}{A - A_0} = \frac{1}{A_\infty - A_0} + \frac{1}{K_{app}(A_\infty - A_0)} \times \frac{1}{[complex]} \quad (2)$$

where,  $A_\infty$  is the absorption when biomolecule was completely saturated via the metal complex solution,  $[complex]$  is the concentration of the Pd(II) complex and  $A_0$  and  $A$  are the absorbance of CT-DNA (at 260 nm) or BSA (at 280 nm) in absence and presence of metal complex. A linear relationship can be acquired between  $1/(A - A_0)$  and the reverse of the complex concentration, then  $K_{app}$  value is obtained from the ratio of the intercept to the slope of this chart [27]. The  $K_{app}$  values for CT-DNA-/BSA-complex systems were used to evaluate the change in the free energy ( $\Delta G^\circ$ ) through the following formula (3):

$$\Delta G^\circ = -RT \ln K_{app} \quad (3)$$

where  $R$  is the ideal gas constant ( $1.987 \text{ cal mol}^{-1} \text{ K}^{-1}$ ) and  $T$  is absolute temperature (300 K).

Second measurement was conducted to follow the biomolecule denaturation via adding different volumes of the Pd(II) complex solution. In this step, 30  $\mu\text{L}$  of CT-DNA stock solution or 450  $\mu\text{L}$  BSA stock solution was reached to the final volume of 2 mL using Tris-HCl buffer. To these blends, 20, 30, 45, ..., 300  $\mu\text{L}$  of metal complex stock solution were added on CT-DNA and 250, 300, 400, ..., 1250  $\mu\text{L}$  on BSA and their patterns were noted at 260 for CT-DNA and at 280 nm for BSA after each injection. For each biomolecule, the absorbance at 640 nm was recorded and then the absorbance values ( $A_{280} - A_{640}$  for BSA and  $A_{260} - A_{640}$  for CT-DNA) were plotted versus the total concentration of the complex.

### 2.7.2. Fluorescence emission titrations

Fluorescence emission experiments were conducted to assess the binding mode of the novel metal complex on CT-DNA and BSA and obtain the thermodynamic parameters. Fluorescence emission of this new complex was checked and observed to be negligible. For the case of DNA, since the amount of fluorescence emission is small, ethidium bromide was added as a fluorescent probe. But, BSA has intrinsically fluorescence because of the presence of tyrosine, tryptophan and phenylalanine residues. To perform titration, the solutions of EB+CT-DNA and BSA were prepared as follows: (i) 90  $\mu\text{L}$  of stock solution of CT-DNA along with 20  $\mu\text{L}$  of EB (0.023 mg/mL) were dissolved in 0.87 mL of Tris-HCl buffer to get the final volume of 0.98 mL, and (ii) 60  $\mu\text{L}$  of stock solution of BSA and 0.94 mL of Tris-HCl buffer were mixed to achieve the final volume of 1 mL. Then for CT-DNA binding, various amounts of Pd(II) complex stock solution (30–160  $\mu\text{L}$ ) was added and titration was performed at 3 temperatures of 293, 300, and 310 K. For BSA, 15–125  $\mu\text{L}$  of Pd(II) stock solution was used to perform titration at the above mentioned temperatures. For both cases, after each addition, the mixture was slowly mixed and maintained 3 min until equilibration and then its spectrum was recorded. These experiments were repeated three times. In these experiments, excitation wavelength for EB+CT-DNA and BSA were taken as 471 and 295 nm, respectively. The fluorescence spectra were measured at the range of 530 to 740 nm for DNA and 310 to 470 nm for BSA. The path length of fluorescence cell was 1 cm and excitation and emission slits were selected both 5 nm. The binding of the metal complex to CT-DNA as well as BSA and subsequent fluorescence quenching mechanism were investigated via Stern-Volmer Eq. (4) [28]:

$$\frac{F_0}{F} = 1 + k_q \tau_0 [Q] = 1 + K_{SV} [Q] \quad (4)$$

where,  $F$  and  $F_0$  are the fluorescence intensities of biomolecule in the presence and absence of metal complex, respectively,  $k_q$  is apparent bimolecular quenching constant,  $\tau_0$  is the average fluorescence lifetime of the fluorophore (EB or BSA) in the absence of

quencher. The  $\tau_0$  value is  $10^{-8}$  s for EB+CT-DNA and BSA [29,30].  $[Q]$  is the Pd(II) complex concentration and  $K_{SV}$  is Stern-Volmer quenching constant. The  $K_{SV}$  values for the case of DNA and BSA were calculated from the slope of  $F_0/F$  plot versus  $[Q]$ .

Then, the binding constant ( $K_b$ ) and number of binding sites per 1000 nucleotides of DNA and/or per molecule of BSA ( $n$ ) were evaluated via plotting  $\log(F_0 - F)/F$  vs.  $\log[Q]$  according to the following formula (5) [31]:

$$\log \frac{F_0 - F}{F} = n \log [Q] + \log K_b \quad (5)$$

Also, thermodynamics parameters ( $\Delta H^\circ$  and  $\Delta S^\circ$ ) were evaluated using van't Hoff equation as follows (6) [32]:

$$\ln K_b = -\frac{\Delta H^\circ}{RT} + \frac{\Delta S^\circ}{R} \quad (6)$$

in Eq. (6),  $T$  is the temperature in kelvin. Finally, the  $\Delta G^\circ$  values were obtained from Eq. (7):

$$\Delta G^\circ = \Delta H^\circ - T \Delta S^\circ \quad (7)$$

These thermodynamic parameters were utilized to estimate the binding modes of Pd(II) complex and biomolecules [33].

### 2.7.3. BSA-FRET

This technique can be utilized to quantify the distance of the bioactive metal complex to the interacted protein molecule, which is a criterion for the interaction between the two. Section 3.5.3 will provide more information regarding this process.

### 2.7.4. CT-DNA gel electrophoresis

Agarose gel electrophoresis was applied for monitoring the effect of  $[\text{Pd}(\text{bpy})(\text{acac})\text{NO}_3]$  on the CT-DNA structure. At the beginning of electrophoresis experiment, four solutions were prepared in 4 different clean tubes, that include separately: tube 1 (30  $\mu\text{L}$  of CT-DNA stock solution and 30  $\mu\text{L}$  Tris-HCl buffer), tube 2 (30  $\mu\text{L}$  CT-DNA, 10  $\mu\text{L}$  complex ( $8 \times 10^{-4}$  M) and 20  $\mu\text{L}$  buffer), tube 3 (30  $\mu\text{L}$  CT-DNA, 15  $\mu\text{L}$  complex and 15  $\mu\text{L}$  buffer) and tube 4 (30  $\mu\text{L}$  CT-DNA, 20  $\mu\text{L}$  complex and 10  $\mu\text{L}$  buffer). All the tubes were blended and left for one night in the refrigerator till the reactions were completed. Afterwards, the solutions were remained for 60 min at 37 °C. 1  $\mu\text{L}$  of loading dye and 9  $\mu\text{L}$  of each sample were mixed and loaded onto a 3% agarose gel. The electrophoresis process was performed in TAE buffer (contains a blend of EDTA, acetic acid and Tris base) at the voltage of 70 V for 60 min. Finally, the gel came out from the buffer tank and was visualized by CCD-5 Gel Documentation System, Iran, using UV light and photographed.

### 2.7.5. Hydrodynamic measurement

Viscosity experiments were performed for different solutions of CT-DNA and Pd(II) complex utilizing Ostwald micro-viscometer (SCHOT-geräte, Germany) at ambient temperature of  $27 \pm 1$  °C. In each sample, the concentration of CT-DNA was kept unchanged (60  $\mu\text{M}$ ) while varying the concentration of Pd(II) complex (0–24  $\mu\text{M}$ ) to attain the ratios of  $r_i = [\text{Pd(II) complex}]/[\text{CT-DNA}] = 0.00, 0.05, 0.10, 0.15, 0.20, 0.25, 0.30, 0.35, 0.40$ . Then, the viscosity measurements were carried out and the flow time was noted four times for each sample with a digital stopwatch and the average value was used for the calculation. The findings were illustrated as  $(\eta/\eta_0)^{1/3}$  against  $r_i$ , where  $\eta$  and  $\eta_0$  are the viscosity of CT-DNA/Pd(II) complex solution and CT-DNA alone, respectively. The relative values of  $\eta/\eta_0$  were achieved by Eq. (8):

$$\frac{\eta}{\eta_0} = \frac{(t_{\text{Pd(II) complex}} - t_0)/t_0}{(t_{\text{CT-DNA}} - t_0)/t_0} \quad (8)$$

where  $t_{\text{Pd(II) complex}}$  and  $t_{\text{CT-DNA}}$  are the average flow time of CT-DNA in presence of palladium(II) complex and CT-DNA alone, respectively.  $t_0$  is related to the buffer [34].

### 2.7.6. BSA-CD spectra

BSA CD spectra (5.5  $\mu\text{M}$ ) with and without  $[\text{Pd}(\text{bpy})(\text{acac})]\text{NO}_3$  complex (different concentration of 0 to 65  $\mu\text{M}$ ) were collected on an AVIV CD spectrometer-model 215, USA. A cylindrical cuvette cell (path length of 1 mm) was applied to perform the measurements in far-UV region (200–250 nm) in a nitrogen atmosphere at 298 K. The CD spectrum of background (working buffer) was subtracted from all CD signals and they were changed to the molar ellipticity and then smoothed via CD software [35,36].

### 2.7.7. Docking protocol

Molecular docking has an extensive diversity of usage in drug discovery and development, including chemical mechanism, structure-activity relationship (SAR), lead optimization, and providing hypotheses to facilitate predictions for studies based on mutagenesis [37]. In order to determine  $\Delta G^0$  and predict the appropriate binding modes and non-covalent molecular binding of new Pd(II) complex with two main biomolecules (DNA and BSA), the molecular docking method was employed. Herein, Auto Dock 4.2 and Auto Dock Tools 1.5.6 programs were utilized for *in-silico* docking procedure. For the representation of the schematic 3D interactions and energy values of each residue, Discovery Studio Visualizer 4.1 was applied. The crystal structures of DNA (PDB ID: 1XRW) octamer 5'-CCTCGTCC-3'/3'-GGAGCAGG-5' and BSA (PDB ID: 4F5S) were obtained from <https://www.rcsb.org/> (Protein Data Bank site). The optimized geometry of the Pd(II) complex was used for docking simulation. The macromolecules structures were initially prepared via eliminating the ligands, water molecules and another monomer (available in BSA structure) and adding polar hydrogens. Then, the Gasteiger and Kollman partial atomic charges were added to the PDB files of the macromolecules and complex structure, respectively. Following the creation of PDBQT files of mentioned structures, they were used as inputs for setting grid boxes. The grid maps along X-, Y- and Z-axis were set to 56, 70 and 50  $\text{\AA}^3$  (0.375  $\text{\AA}$  grid spacing) for DNA and 70, 70 and 70  $\text{\AA}^3$  with the same grid spacing for both drug binding sites of BSA, utilizing Auto Grid program. LGA (Lamarckian genetic algorithm) was implemented for 10 number of runs [38,39]. Maximum numbers of generations and fitness evaluations were fixed to 27,000 and 2,500,000, respectively. Default values were used for other parameters. Chimera 1.11.2 software was used for visualizing the output of docked poses.

## 3. Results and discussion

A novel and bioactive Pd(II) complex of general formula  $[\text{Pd}(\text{bpy})(\text{acac})]\text{NO}_3$  was prepared through precipitating the chloride ions from  $[\text{Pd}(\text{bpy})\text{Cl}_2]$  complex via silver(I) nitrate in presence of acac-NaOH blend. This compound is yellow solid and water or Tris-HCl buffer-soluble, being the first serious step towards future usage in biological systems. We have attempted to obtain a single crystal ideal for X-Ray experiment, but have not yet been successful. However, satisfactory structural findings were acquired from various spectroscopic (FT-IR,  $^1\text{H}$  NMR and UV-Vis) and non-spectroscopic procedures including elemental analysis and conductivity measurement (complex is of good purity) as well as DFT calculations. The results of experimental and computational methods are aligned with those of the suggested structure. On the other hand, the lipophilicity determination of the novel metal complex was checked in term of log P. *In-vitro* cytotoxicity of the complex was checked by investigating it against K562 cells. In-detailed biomolecular interaction studies of the complex were investigated. In all interaction experiments, we found no any spectral changes occur after three minutes of injecting the Pd(II) complex solution to CT-DNA or BSA solutions. In this way we found out time du-

ration or incubation time to be the three minutes. The finding of these above approaches are discussed below:

### 3.1. Structural characterization of $[\text{Pd}(\text{bpy})(\text{acac})]\text{NO}_3$

$[\text{Pd}(\text{bpy})(\text{acac})]\text{NO}_3$  is yellow color, while both of its ligands are colorless. It melts/decomposes at higher temperature (226–227  $^\circ\text{C}$ ) than that of respective ligands (bpy = 70–73  $^\circ\text{C}$  and acac = –23  $^\circ\text{C}$ ). These are two indications of the formation of the complex. The theoretical results calculated for palladium (25.06), carbon (42.55), hydrogen (3.55) and nitrogen (9.93) contents (%) were found to be in favor to experimental values obtained (Pd = 25.00, C = 42.38, H = 3.50 and N = 9.94%). The molar conductance value of the above Pd(II) complex in double distilled water ( $10^{-4}$  M) was 144  $\Omega^{-1} \text{mol}^{-1} \text{cm}^2$  illustrating the complex is 1:1 electrolyte [40] and a rough support that both ligands are bidentate chelates. Further support that Pd(II) ion is coordinated to both oxygen atoms of acetylacetonato and two nitrogen atoms of 2,2'-bipyridine comes from the findings obtained from UV-Vis, FT-IR and  $^1\text{H}$  NMR spectra of the metal complex.

In the FT-IR pattern of free acetylacetonato ligand, 2 characteristic bands have been reported [41] at 1729  $\text{cm}^{-1}$  and 1622  $\text{cm}^{-1}$ . These bands are attributed to the ketonic and enolic stretching frequencies of the C=O groups, respectively. In the Pd(II) complex, only one band at 1547  $\text{cm}^{-1}$  was observed which shows coordination of acac ligand as bidentate chelate [42,43]. This is because of coordination, the negative charge on acac is delocalized on both C=O groups present in the chelate ring and thus spectrum shows a single stretching frequency due to both resonated CO groups. The intense and sharp stretching peak that appeared at 1383  $\text{cm}^{-1}$  in the spectrum of  $[\text{Pd}(\text{bpy})(\text{acac})]\text{NO}_3$  is assigned to  $\text{NO}_3^-$  ion, showing that this group is present as counter ion and not coordinated one [44].

$^1\text{H}$  NMR pattern of  $[\text{Pd}(\text{bpy})(\text{acac})]\text{NO}_3$  complex was measured in DMSO- $d_6$  using TMS as standard reference. In this pattern, two sets of resonance signals were observed. In the first set, two sharp signal resonating at 2.1 and 5.7 ppm are assigned to  $\text{H}_F$  (6H) and  $\text{H}_E$  (1H) of acac moiety (see Fig. 2). The second set signals are attributed to the protons of coordinated 2,2'-bipyridine moiety. These doublet signals resonate at 7.8 (2H), 8.31 (2H), 8.37 (2H) and 8.60 ppm (2H), which are assigned to  $\text{H}_B$ ,  $\text{H}_C$ ,  $\text{H}_D$  and  $\text{H}_A$ , respectively (Fig. 2). The integration area under these signals are in the ratio of 6: 1: 2: 2: 2 ( $\text{H}_F$ :  $\text{H}_E$ :  $\text{H}_B$ :  $\text{H}_C$ :  $\text{H}_D$ :  $\text{H}_A$ ), support the protons of coordinated acac and bpy moieties to the Pd(II) center.

In the electronic absorption spectrum of  $[\text{Pd}(\text{bpy})(\text{acac})]\text{NO}_3$  in  $\text{H}_2\text{O}$ , there are three broad absorption bands at 308 nm ( $\epsilon = 17,354$ ), 234 ( $\epsilon = 29,580$ ) and 205 ( $\epsilon = 58,540$ ) which are assigned to  $\pi \rightarrow \pi^*$  and  $n \rightarrow \pi^*$  transitions within organic ligands as well as  $\text{NO}_3^-$  ion that show overlapping and thus could not be separated.

The above characterization results of conductivity measurement, elemental analysis,  $^1\text{H}$  NMR, UV-Vis and FT-IR are in accordance with the proposed structure given in Fig. 2.

### 3.2. Theoretical approaches

#### 3.2.1. Geometry optimization

The optimized molecular geometry of the Pd(II) complex was evaluated via Gaussian09 program and is demonstrated in Fig. 3(a) along with some selected bond angles and lengths demonstrated in the figure. Since, the X-ray diffraction (XRD) of this complex is not yet reported so we checked the validity of our quantum mechanical results with XRD data of similar complexes [45,46]. We found a good agreement between our computational results with the reported XRD data.

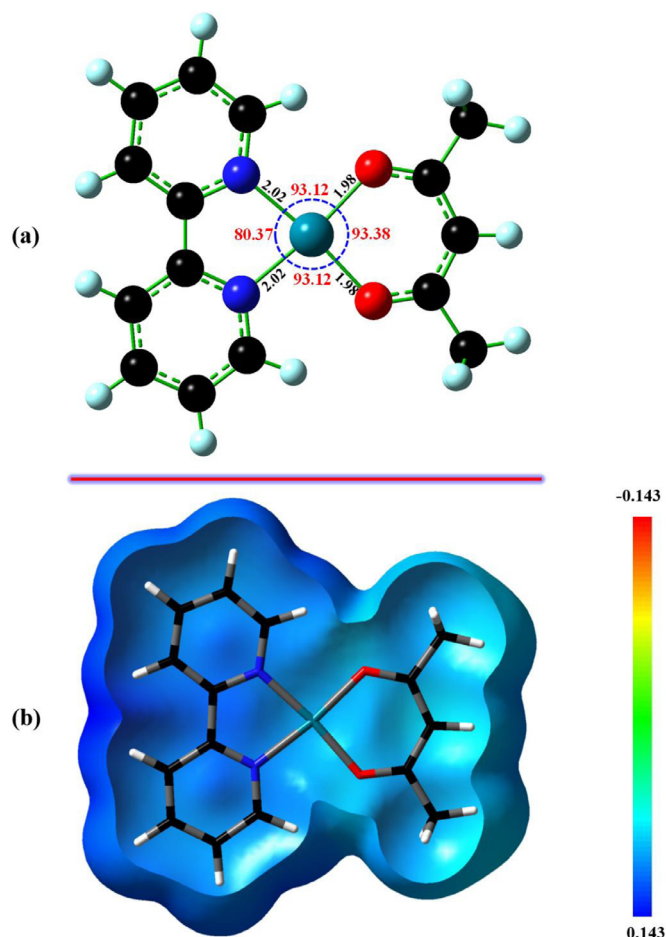


Fig. 3. (a) Optimized geometry and (b) Cut from MEP plot of Pd(II) complex.

### 3.2.2. MEP analysis

MEP is relevant to the electronic density and illustrates the charge distribution within the surface of chemical system. The electrostatic potential is an appropriate approach for analyzing processes like drug-receptor interactions which are based on the recognition of the drug compound by the macromolecule because it is via their electrostatic potentials that they first feel each other [47]. In order to investigate the reactive regions of nucleophilic and electrophilic attacks along with hydrogen bonding for Pd(II) complex, MEP calculation was performed for the optimized geometry.

Fig. 3(b) demonstrates the electrostatic potential contour map of the investigated complex. In this figure, the colors grading is used to show different values of the electrostatic potential. Red and blue color represents the most electronegative (rich in electron) and electropositive (poor in electron) sites of compound, respectively. For this compound the light blue shade corresponds to the negative electrostatic potential and dark blue is related to the positive electrostatic potential. Negative potential sites generally correspond to the free electron pair of electronegative atoms. The MEP map illustrates that the negative charge covers acac ligand and the positive area is over the bpy rings. The more electronegativity in the C=O groups of acac ligand makes it the most reactive part of the molecule for electrophilic attacks and can also act as an electron donor in hydrogen bond interactions.

### 3.2.3. FMO analysis

The HOMO (highest occupied molecular orbital) energy shows the tendency to donate an electron while the LUMO (lowest unoccupied molecular orbital) energy demonstrates the capability to

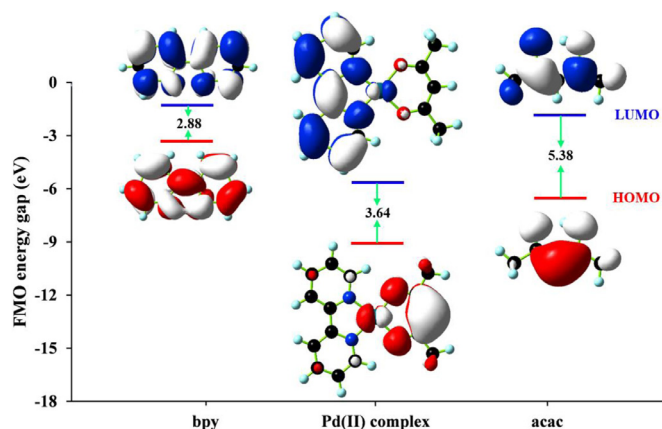


Fig. 4. HOMO (lower) and LUMO (upper) plots of Pd(II) complex, bpy and acac.

accept an electron. The frontier molecular orbitals, HOMO and LUMO, ascertain how a compound interacts with other molecules and specify its stability and reactivity. For the purpose of drug design, different new chemical reactivity descriptors including electron affinity, global hardness, ionization energy, electrophilicity and chemical potential were introduced. By having FMO energies, the first ionization energy ( $I$ ) and first electron affinity ( $A$ ) can be determined as:  $I = -E_{\text{HOMO}}$ ,  $A = -E_{\text{LUMO}}$  [48]. The hardness ( $\eta$ ), chemical potential ( $\mu$ ) and global electrophilicity ( $\omega$ ) are expressed via the following relations:  $\eta = (E_{\text{LUMO}} - E_{\text{HOMO}})/2$ ,  $\mu = (E_{\text{LUMO}} + E_{\text{HOMO}})/2$  and  $\omega = \mu^2/2\eta$ , respectively [49–51]. The hardness signifies the resistance of compound for polarization during the chemical process and the deformation of electron cloud. Hard molecules are small with low polarizability and soft molecules are large and polarizable. The negative value of chemical potential implies that the compound is stable. Electrophilicity ( $\omega$ ) descriptor represents the stabilization in energy when the compound obtains an electron from other species.

The HOMO and LUMO diagrams of the compounds are represented in Fig. 4. As can be seen in this figure, HOMO is localized over transition metal and acac ligand, while the LUMO is localized over transition metal and bpy. Consequently, the HOMO→LUMO transition involves the transfer of electron density from acac to bpy ligand. This demonstrates that charge transfer happens within the complex through the conjugation. For the newly made complex and its related ligands,  $E_{\text{HOMO}}$ ,  $E_{\text{LUMO}}$ , energy gap ( $\Delta E = E_{\text{LUMO}} - E_{\text{HOMO}}$ ),  $I$ ,  $A$ , global hardness ( $\eta$ ), global electrophilicity ( $\omega$ ) and chemical potential ( $\mu$ ) are listed in Table 1. It is clear that the chemical potential of Pd(II) complex is negative and lower than that of both ligands, so it is stable and does not decompose spontaneously to its initial elements. The hardness value of [Pd(bpy)(acac)]NO<sub>3</sub> is higher than that of bpy and lower than acac. Since it has a moderate value of hardness and kinetic stability so it is reactive and has enough polarizability to interact with another species like macromolecules.

### 3.3. Solution stability and partition coefficient (log $P$ )

The stability of molecules being a momentous feature affecting their clinical usages in medicine. Therefore, the stability of Pd(II) complex in aqueous solutions (water and Tris-HCl buffer) was investigated at 37 °C through electronic absorption measurements before performing biological tests. According to the obtained results, no alteration in the absorption spectra of the complex was observed (supplementary Fig. S1). This complex remained stable in aqueous solutions over the period of time, which illustrates that

**Table 1**  
Quantum chemical descriptors of Pd(II) complex, bpy and acac (the values are given in eV).

Compound	$E_{\text{HOMO}}$	$E_{\text{LUMO}}$	$\Delta E$	I	A	$\eta$	$\mu$	$\Omega$
Pd(II) complex	-9.54	-5.90	3.64	9.54	5.90	1.82	-7.72	16.37
bpy	-3.64	-0.76	2.88	3.64	0.76	1.44	-2.20	1.68
acac	-6.73	-1.35	5.38	6.73	1.35	2.69	-4.04	3.03

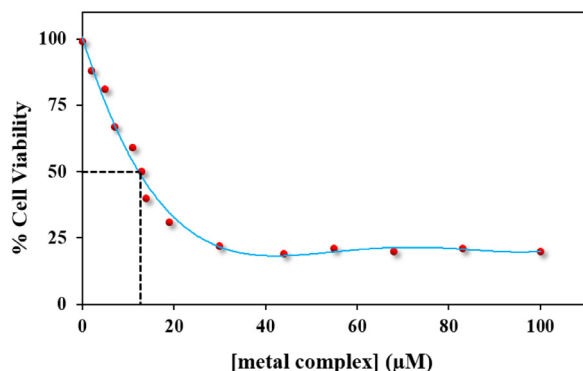


**Fig. 5.** Diagram representing the effect of  $[\text{Pd}(\text{bpy})(\text{acac})]\text{NO}_3$  complex on K562 leukemia cell line.

no dissociation happens when utilizing doubly distilled water or Tris-HCl buffer to dissolve the complex.

Lipophilicity is a prominent factor which is used in drug design and discovery process. It is generally accepted to be the desire of nonpolar compounds to form aggregates to decrease their contact surface with the polar compounds such as water. Hydrophobic interactions, the initial driving force in many phenomena, are some of the main interactions in the nature [52]. High lipophilic compounds can easily penetrate to the cell membrane and access the tissue without difficulty. As described in the experimental section the lipophilic behavior of the Pd(II) complex is evaluated in terms of log P utilizing n-octanol/water system. Here, the obtained value of log P for the newly made Pd(II) complex is  $-0.85 \pm 0.03$ . Furthermore, the known value of log P for cisplatin reported in the literature is  $-2.28 \pm 0.07$  [53]. Also, the lipophilicity values of most anticancer compounds are between  $-0.4$  to  $5.6$  (in average  $2.52$ ) [54]. However, the lipophilicity of the complex reported in this article and the well-known anticancer drug, cisplatin, follows the order complex > cisplatin. This higher lipophilicity character of the  $[\text{Pd}(\text{bpy})(\text{acac})]\text{NO}_3$  in compare to that of cisplatin supports its cytotoxicity potency (see Section 3.4.) and vis versa. In the other word, higher lipophilicity suggests that the title compound can pass through the cell membrane more easily which leads to an increase in its concentration within the cells. Therefore, the complex may have a better cytotoxic character than cisplatin.

### 3.4. Cytotoxicity experiment

The novel  $[\text{Pd}(\text{bpy})(\text{acac})]\text{NO}_3$  complex has been measured for its *in-vitro* cytotoxicity versus K562 cell line via MTT measurement. The cells were incubated for 24 h with various complex concentrations (0–100  $\mu\text{M}$ ). The result of cytotoxicity was plotted as the percentage of cell viability against concentration of the complex ( $\mu\text{M}$ ), which is shown in Fig. 5. As demonstrated in Fig. 5, the cell viability was decreased after addition of diverse concentrations of  $[\text{Pd}(\text{bpy})(\text{acac})]\text{NO}_3$  and  $\text{IC}_{50}$  was determined. According to Fig. 5, the evaluated  $\text{IC}_{50}$  value of the newly made complex is  $13 \mu\text{M}$  at incubation time of 24 h. So,  $\text{IC}_{50}$  value of the anticancer agent, cisplatin, under the similar experimental conditions was detected  $154 \mu\text{M}$  [55], which is much higher in compared with the  $\text{IC}_{50}$  value of  $[\text{Pd}(\text{bpy})(\text{acac})]\text{NO}_3$  complex. This growth inhibition not

only shows antitumor potency of the agent, but also indicates its probable interaction with K562 cells DNA and thus encouraged us to prove the later by detailed DNA-binding studies.

### 3.5. Macromolecules binding studies

#### 3.5.1. UV-Vis titrations

UV-Vis spectroscopy is a critical and fundamental technique to investigate the binding tendency of metal based drugs during drug-macromolecule (DNA or protein) interaction, as the affinity to macromolecule causes the electronic perturbations in their UV patterns [56,57]. These perturbations affect the location and maximum intensity of related peak and includes the following types: hypsochromic (blue shift), bathochromic (red shift), hypochromic (decreasing intensity) and hyperchromic (increasing intensity) [58]. Generally, for the case of DNA, hypochromic along with the red shift is related to the intercalation of metal complex through strong  $\pi$ - $\pi$  interaction with the base pairs of DNA, while hyperchromism along with the blue shift is universally attributed to the groove binding. Moreover, partial intercalation for complexes with large functional groups in their structures and without complete intercalation capability leads to hypochromism without any considerable red shift. Surface interaction was demonstrated to cause a small absorbance decrease with no notable shift in maximum wavelength [59–61]. Fig. 6 illustrates the absorption spectra of CT-DNA and BSA titrated with different volumes of  $[\text{Pd}(\text{bpy})(\text{acac})]\text{NO}_3$  complex (20 to 300  $\mu\text{L}$  from complex stock solution for CT-DNA and 250 to 1250  $\mu\text{L}$  for BSA, respectively). From Fig. 6, it is clear that the peak intensity of CT-DNA or BSA decreases with raising complex concentration, while,  $\lambda_{\text{max}}$  in Fig. 6(a) shifts towards the larger wavelengths. These results represent the binding affinities of  $[\text{Pd}(\text{bpy})(\text{acac})]\text{NO}_3$  to CT-DNA or BSA [62,63]. On the other hand, the calculated hypochromicity for CT-DNA and BSA-complex systems were 32.17% and 38.67% respectively with a red shift of 4 nm for CT-DNA binding system. As a result, intercalation binding mode is recommended relating to the binding of synthesized Pd(II) complex with duplex of DNA. Generally, compounds containing fused aromatic rings are proper to intercalate into the duplex of DNA through inserting their planar functional groups between the base pairs of DNA, while those possess unfused aromatic rings can discover desired orientation for binding to the groove sites of DNA [64,65]. The aromatic fused ring of  $[\text{Pd}(\text{bpy})(\text{acac})]\text{NO}_3$  complex i.e. bpy ligand is able to be inserted between the bases pairs of DNA via intercalation binding mode.

For quantitative comparison,  $K_{\text{app}}$  for CT-DNA/BSA-complex systems were also calculated utilizing Eq. (2) as summarized in Table 2 (Fig. 6, insets). The calculated  $K_{\text{app}}$  of  $[\text{Pd}(\text{bpy})(\text{acac})]\text{NO}_3$  complex to CT-DNA was found to be a bit higher than that of EB ( $K_{\text{b}} = 1.23 \times 10^5 \text{ M}^{-1}$ ) [66]. These findings demonstrate that probably interaction mode of  $[\text{Pd}(\text{bpy})(\text{acac})]\text{NO}_3$  complex to CT-DNA should be intercalation similar to that of classical intercalator (EB). On the other hand, the binding affinities of  $[\text{Pd}(\text{bpy})(\text{acac})]\text{NO}_3$  to CT-DNA ( $K_{\text{app, CT-DNA}} = 2.35 \times 10^5 \text{ M}^{-1}$ ) is much higher than that of BSA ( $K_{\text{app, BSA}} = 1.73 \times 10^3 \text{ M}^{-1}$ ) indicating that this complex has less interaction affinity in compare to CT-DNA and thus no abrupt structural damage of BSA is expected [67]. The  $\Delta G^\circ$  values of the complex-CT-DNA and -BSA binding systems at 300 K were obtained to be  $-7.37$  and  $-4.45$  Kcal/mol, respectively, which

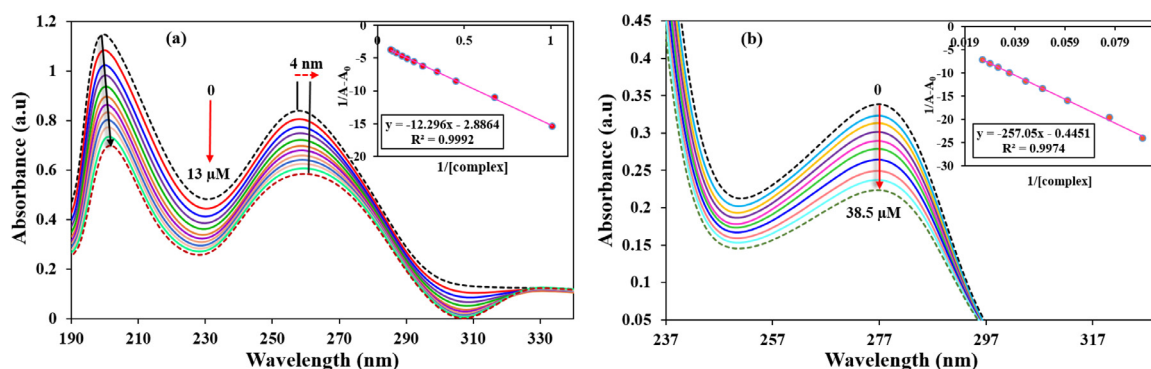


**Fig. 6.** Absorption patterns of CT-DNA (a) and BSA (b) in the absence and presence of increasing concentrations of  $[\text{Pd}(\text{bpy})(\text{acac})]\text{NO}_3$ , [CT-DNA] =  $127 \mu\text{M}$ , [BSA] =  $8.2 \mu\text{M}$  and [complex] = 0.00 –  $13.00 \mu\text{M}$  for CT-DNA and 0.00 –  $38.50 \mu\text{M}$  for BSA at  $T = 300 \text{ K}$ . insets illustrate the outline of  $1/(A-A_0)$  vs.  $1/[\text{complex}]$  for CT-DNA and BSA respectively to calculate  $K_{\text{app}}$  values.

**Table 2**

The evaluated binding parameters from UV-Vis spectroscopic method for the interaction of  $[\text{Pd}(\text{bpy})(\text{acac})]\text{NO}_3$  complex with CT-DNA and BSA.

	T (K)	$K_{\text{app}}$ ( $\text{M}^{-1}$ )	$[\text{L}]_{1/2}$ (mM)	$\Delta G^\circ$ (Kcal/mol)	$H^\circ$ (%)
<b>CT-DNA binding</b>	300	$2.35 \times 10^5$	0.0048	-7.37	32.17
<b>BSA binding</b>	300	$1.73 \times 10^3$	0.023	-4.45	38.67

\*  $H$  = percentage hypochromicity.

demonstrate spontaneous binding between this complex and both biomolecules.

In addition, the reduction in the absorption patterns of CT-DNA and BSA upon increasing concentration of Pd(II) complex demonstrates that a type of conformational alteration in the primitive structure of biomolecules occur. The absorbing components in the native structure of DNA (pyrimidine and purine bases) and BSA (R groups attached to amino acid residues) make above changes via hiding from the UV waves, causing a decrement in the intensity of electronic absorption patterns with increasing concentration of  $[\text{Pd}(\text{bpy})(\text{acac})]\text{NO}_3$  [68]. These classes of conformational alterations may be attributed to CT-DNA or BSA refolding.

In the second experiment, the profile of alterations in the patterns of absorbance at 260 nm for CT-DNA and 280 nm for BSA were plotted versus the concentrations of the complex (Fig. 7). From the analysis of this graph, we are able to obtain a crucial parameter ( $[\text{L}]_{1/2}$ ). This parameter denotes the complex concentration at the midpoint of the transition of biomolecule from primary structure to deformed conformation. As Fig. 7 illustrates, the obtained values of  $[\text{L}]_{1/2}$  in the binding between  $[\text{Pd}(\text{bpy})(\text{acac})]\text{NO}_3$  and CT-DNA and BSA are 0.0048 and 0.023 mM, respectively.

The obtained results from absorption experiments are: 1)  $[\text{Pd}(\text{bpy})(\text{acac})]\text{NO}_3$  complex leads to the conformation alterations

in the native structure of CT-DNA and BSA at very low concentration, 2) the  $[\text{L}]_{1/2}$  values for the above metal complex in CT-DNA binding is lower than BSA binding, indicating that if this complex is applied as a potential antitumor agent, its antitumor attributes is high (due to potent binding to CT-DNA) and its side effects is probably low (due to weak binding to BSA).

The above discussion is complemented by the two following paragraphs:

Binding constant in the interaction of the complex with DNA ( $2.35 \times 10^5$ ) and BSA ( $1.73 \times 10^3$ ) (Table 2) tells us that interaction affinity with DNA is more than that of BSA. From the other side, since we have not done *in-vivo* studies, one can just say: High interaction affinity may cause halting DNA- duplication leading to cancer cell death. While low interaction affinity with BSA possibly bring about the reversibility binding behavior of BSA with the complex which is necessary for uploading in BSA and releasing near the target cells.

In the cell (cuvette), where interaction is carried out, the interfering molecules may be NaCl or Tris- HCl buffer only. Thus, UV-Vis spectra of the Pd(II) complex, CT-DNA and BSA were recorded in i) deionized water ii) in 10 mM Tris- HCl buffer solution of pH = 7.2 and iii) in 10 mM NaCl solution (i.e. about the same concentration in the blood stream). All the three showed exactly

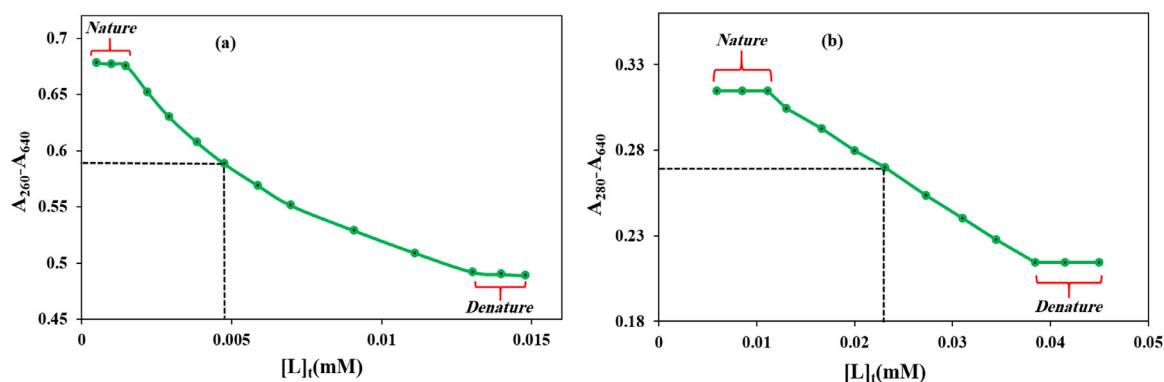


**Fig. 7.** The decrease in the absorbance of CT-DNA at 260 nm (a) and BSA at 280 nm (b) upon increasing the concentration of  $[\text{Pd}(\text{bpy})(\text{acac})]\text{NO}_3$  at 300 K.

**Table 3**

Comparison of  $K_{app}$ ,  $L_{1/2}$  and  $IC_{50}$  values found for  $[Pd(bpy)(acac)]NO_3$  with its structurally related compounds found from the literature.

compound	$K_{app, DNA}$ ( $M^{-1}$ )	$K_{app, BSA}$ ( $M^{-1}$ )	$L_{1/2, DNA}$ ( $\mu M$ )	$L_{1/2, BSA}$ ( $\mu M$ )	$IC_{50}$ ( $\mu M$ )	Reference
$[Pd(bpy)(acac)]NO_3$	$2.35 \times 10^5$	$1.73 \times 10^3$	4.8	23	13	
$[Pd(phen)(acac)]NO_3$	$2.87 \times 10^5$	$1.37 \times 10^3$	3.84	28.57	18	[26]
$[Pd(bpy)(SA)]$	$3.90 \times 10^4$	–	18	–	36	[68]
$[Pd(bpy)(SSA)]$	$1.09 \times 10^5$	–	13	–	27	[68]

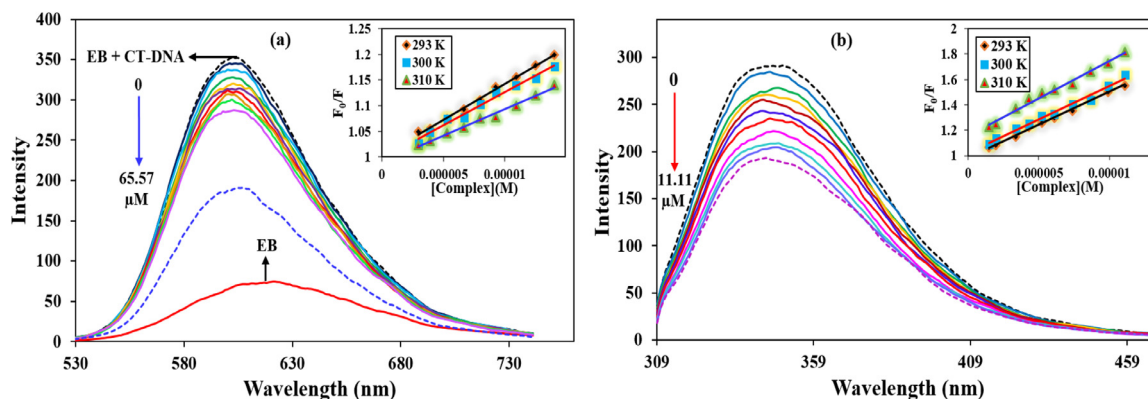


**Fig. 8.** The emission spectra of interacted EB+CT-DNA (a) and intrinsic fluorescence of BSA (b) in the absence and presence of the  $[Pd(bpy)(acac)]NO_3$  complex (0.00, 2.97, 3.92, 5.31, 6.67, 7.98, 9.26, 10.90, 12.50, 14.00 and 65.57  $\mu M$  of stock solution for CT-DNA and 0.00, 1.48, 1.96, 3.38, 4.30, 5.21, 6.10, 7.41, 8.67, 9.91 and 11.11  $\mu M$  for BSA) at 300 K. Insets show Stern-Volmer plots for binding of EB+CT-DNA (a, inset) and BSA (b, inset) to  $[Pd(bpy)(acac)]NO_3$  complex.

the same spectral pattern, indicating that NaCl and Tris- HCl buffer structurally do not interfere with the Pd(II) complex, CT-DNA and BSA solutions. However, we have not checked the interfering effect of other molecules or ions.

It is noteworthy here to compare UV-Vis and cytotoxicity studies of the Pd(II) complex under investigation with structurally related compounds available in the literature:  $[Pd(bpy)(acac)]NO_3$  bears N-N and O-O donor ligands, similar to that of well-known anticancer drug, carboplatin (Fig. 1). In these type of compounds, the N-N donor ligands are ancillary and the O-O donor are leaving groups, which can get substituted with biomolecules like DNA. There are many O-O bonded metal complexes in the literature. However, for few of them the same experiments had been carried out as we did in present paper. These finding results for structurally related metal complexes include:  $K_{app}$ ,  $L_{1/2}$  and  $IC_{50}$  and are gathered in Table 3.

As the data in Table 3 shows, there are no proper trends in the values of  $K_{app}$  and  $L_{1/2}$ . However,  $IC_{50}$  value of  $[Pd(bpy)(acac)]NO_3$  is the lowest, indicating higher *in-vitro* activity of this compound.

### 3.5.2. Fluorescence titration studies

Fluorescence titration technique was utilized to understand the type of the complex interactions with EB+CT-DNA and BSA at temperatures of 293, 300, and 310 K. The fluorescence spectra of EB+CT-DNA and BSA in presence of Pd(II) complex are illustrated in Fig. 8(a and b). Fig. 8(a) shows by addition of more amount of complex, a smooth reduction in the emission intensity of EB+CT-DNA is observed without even any noticeable change in the peak position. It has been confirmed that if the fluorescence intensity of the EB+DNA in presence of a given compound decreases more than 50% and the ratio of complex concentration to DNA is less than 100, then it is assumed that they interact via intercalation [69]. In this work, the addition of  $[Pd(bpy)(acac)]NO_3$  caused a considerable reduction in the emission intensity of the EB+CT-DNA system at the end of titration (50.0%, Fig. 8(a)), which indicates that this complex is probably bound to CT-DNA in a similar mode to EB, i.e., intercalation mode.

Fig. 8(b) illustrates that the BSA emission spectra reduce in the presence of complex without sudden alteration in the location of maximum emission peak. In the other word, the interaction of the  $[Pd(bpy)(acac)]NO_3$  to the BSA diminishes the inherent fluorescence ascribed primarily to the Tyr, Phe-and particularly Trp-residues of BSA. This means the interaction of Pd(II) complex with BSA causes some conformational changes in hydrophobic environment around tryptophan residues of BSA and leads to the reduction in emission intensity of BSA.

Quenching is a procedure in which the emission intensity of a fluorophore substance reduces due to one of the following reasons: formation of non-fluorescent complex in the ground state (static quenching), the collision of given substance and fluorophore in the excited state which leads to the energy transfer between them (dynamic quenching). In static quenching, increasing temperature leads to the decrease in complex formation and therefore decreasing the Stern-Volmer constants. While in dynamic quenching raising temperature causes more collision between fluorophore and quencher and increases quenching and Stern-Volmer constants. Using fluorescence emission data, the  $K_{SV}$  and  $k_q$  values were determined and summarized in Table 4 for biomolecules interaction. The results in this table for DNA shows that with increasing temperature,  $K_{SV}$  reduces and the  $k_q$  values are greater than maximal dynamic quenching constant ( $2 \times 10^{10} M^{-1}s^{-1}$ ). It could be concluded that the fluorescence quenching mechanism in the binding of  $[Pd(bpy)(acac)]NO_3$  to CT-DNA is likely to be static quenching. In addition, the obtained results for BSA demonstrate that with increasing temperature,  $K_{SV}$  increases which implies the quenching mechanism is dynamic. Furthermore, the values of  $k_q$  are greater than  $2 \times 10^{10} M^{-1}s^{-1}$  which confirms static quenching. Therefore, the fluorescence quenching mechanism of interaction between BSA and  $[Pd(bpy)(acac)]NO_3$  is a combination of static and dynamic. Such a quenching mechanism was observed for the reported Pd(II) complexes [26,68]. Although, the linear relation between  $F_0/F$  and  $[complex]$  (as illustrated in the inset of Fig. 8) and the increase in  $K_{SV}$  value with rising temperature shows that the dominant quenching mechanism is dynamic [70,71].

**Table 4**

Stern-Volmer constants, bimolecular quenching rate constants, binding constants, number of binding sites and thermodynamic parameters of [Pd(bpy)(acac)]NO<sub>3</sub> with CT-DNA and BSA at different temperatures.

	T (K)	$K_{sv} \times 10^4$ (M <sup>-1</sup> )	$k_q \times 10^{12}$ (M <sup>-1</sup> s <sup>-1</sup> )	$K_b \times 10^4$ (M <sup>-1</sup> )	$n$	$\Delta G^\circ$ (kcal/mol)	$\Delta H^\circ$ (kcal/mol)	$\Delta S^\circ$ (kcal/K.mol)
CT-DNA binding	293	1.41 ± 0.02	1.41 ± 0.02	1.20 ± 0.04	0.99 ± 0.02	-5.46 ± 0.09	15.37 ± 0.07	0.07 ± 0.002
	300	1.30 ± 0.02	1.30 ± 0.02	2.14 ± 0.05	1.05 ± 0.01	-5.96 ± 0.07		
	310	1.04 ± 0.03	1.04 ± 0.03	5.09 ± 0.04	1.15 ± 0.03	-6.67 ± 0.07		
BSA binding	293	5.17 ± 0.03	5.17 ± 0.03	14.00 ± 0.04	1.09 ± 0.02	-6.90 ± 0.05		
	300	5.26 ± 0.02	5.26 ± 0.02	1.60 ± 0.04	0.90 ± 0.02	-5.83 ± 0.05	-51.73 ± 0.06	-0.15 ± 0.001
	310	5.87 ± 0.03	5.87 ± 0.03	0.10 ± 0.04	0.63 ± 0.01	-4.30 ± 0.04		

All results were expressed as the mean ± standard deviation of three independent experiments.

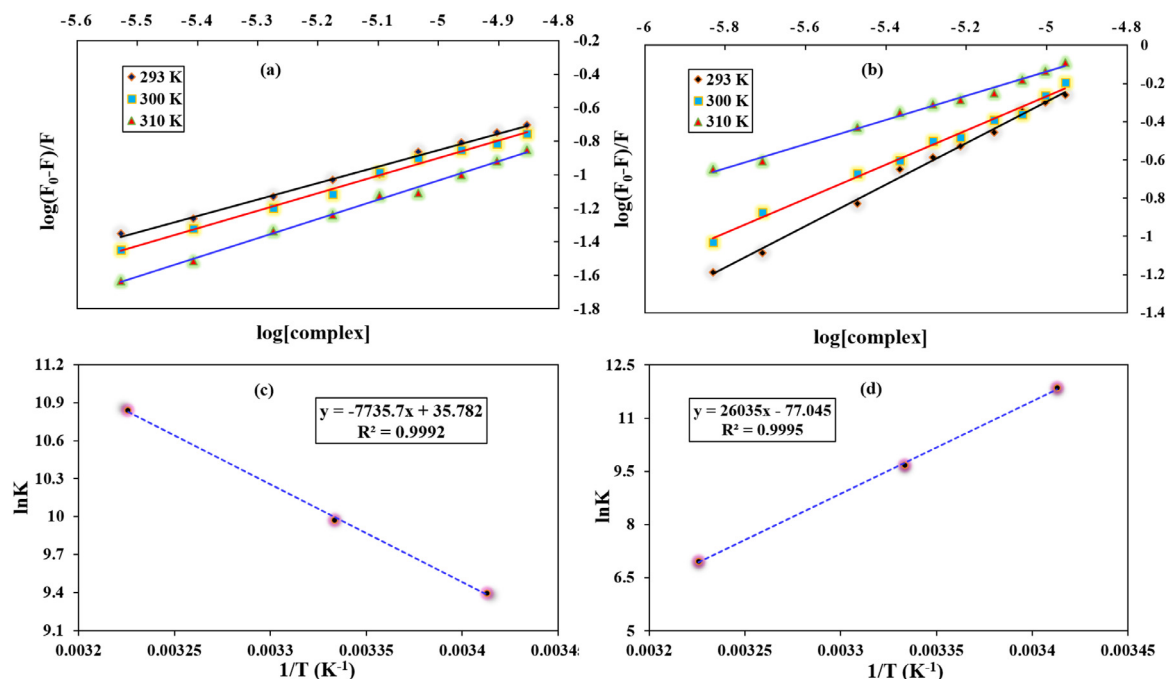


**Fig. 9.** The plot of  $\log(F_0 - F)/F$  vs.  $\log[\text{complex}]$  for the CT-DNA-[Pd(bpy)(acac)]NO<sub>3</sub> system (a) and BSA-[Pd(bpy)(acac)]NO<sub>3</sub> system (b) at three temperatures (293, 300, and 310 K). Van't Hoff plot for the interaction of CT-DNA (c) and BSA (d) with [Pd(bpy)(acac)]NO<sub>3</sub> complex at three various temperatures.

Utilizing Eq. (5) and titration data, the binding constants ( $K_b$ ) and number of binding sites on biomolecules were evaluated. Fig. 9(a and b) demonstrate the plots of  $\log(F_0 - F)/F$  against  $\log[Q]$  for CT-DNA and BSA binding, respectively. Then, the  $K_b$  and  $n$  values were calculated from the intercept and slope of these plots, respectively. The values of  $K_b$  and  $n$  for [Pd(bpy)(acac)]NO<sub>3</sub> at three temperatures are specified in Table 4 for biomolecules interaction. As can be seen in this table, the binding constant of complex with CT-DNA increases with raising temperature which confirms that the formation of complex-CT-DNA system is more favorable at higher temperatures. In contrast, for BSA interaction with increasing temperature, the  $K_b$  values decreases. This shows the interaction between metal complex and BSA is exothermic. Furthermore, the  $n$  value is ~1, demonstrating that there is only one interaction site on BSA and CT-DNA for [Pd(bpy)(acac)]NO<sub>3</sub> complex.

Utilizing Eqs. (6) and (7) and the values of  $K_b$ , the thermodynamic parameters were determined. They can be utilized to estimate the essence of driving forces of the complex and EB+CT-DNA/BSA. These forces are electrostatic, hydrophobic, van der Waals interactions and hydrogen bond. Fig. 9 (c and d) show the plot of  $\ln K_b$  against  $1/T$  based on the formula (6) for EB+CT-DNA and BSA, respectively. The  $\Delta S^\circ$  and  $\Delta H^\circ$  values were determined using the intercept and slope of these plots. The changes in binding free energy,  $\Delta G^\circ$ , were obtained using Eq. (7) for both systems. The values of thermodynamic parameters are mentioned in Table 4 for biomolecules interaction. Yang et al. concluded that the sign of the

thermodynamic quantities and type of interactions are correlated [72] as follows:  $\Delta H^\circ < 0$  and  $\Delta S^\circ < 0$  show hydrogen bonds and van der Waals forces,  $\Delta H^\circ > 0$  and  $\Delta S^\circ > 0$  refer to hydrophobic interactions and  $\Delta H^\circ < 0$  and  $\Delta S^\circ > 0$  indicate electrostatic interactions. In this study,  $\Delta H^\circ < 0$  and  $\Delta S^\circ < 0$  for BSA binding indicate that the forces holding [Pd(bpy)(acac)]NO<sub>3</sub> complex with BSA are hydrogen bond and van der Waals forces. Moreover,  $\Delta H^\circ > 0$  and  $\Delta S^\circ > 0$  for DNA binding illustrates that the obtained CT-DNA-Pd(II) complex adduct is stabilized mainly by hydrophobic interactions. Same results have been observed for the structurally analogous Pd(II) complexes [26,68]. As shown in Table 4 the  $\Delta G^\circ$  values are negative. Hence, the formation of CT-DNA-/BSA-Pd(II) complex are spontaneous process [73,74].

### 3.5.3. FRET calculation

distance-dependent binding between the various electronic excited states of compounds is called fluorescence resonance energy transfer, which is one of the most widely used techniques for measuring the distance between drug and protein in a complex. This procedure permits the excitation energy to be transferred from a donor compound to an acceptor compound without emission of a photon from donor molecular system [75]. The procedure is also known as Förster's resonance energy transfer. FRET expresses the energy transfer efficiency ( $E$ ) as follows [76]:

$$E = 1 - \frac{F}{F_0} = \frac{R_0^6}{R_0^6 + r^6} \quad (9)$$

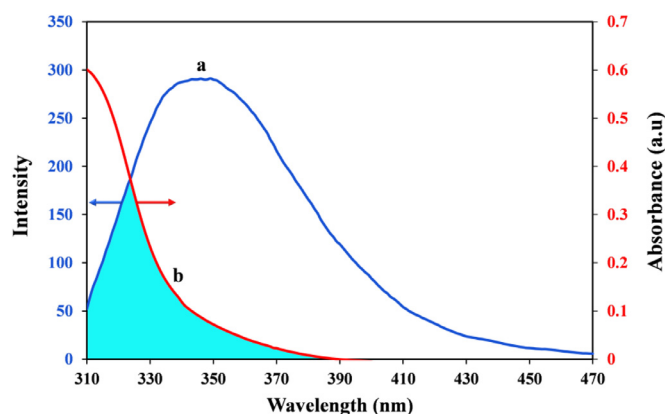


**Fig. 10.** Overlap of the fluorescence emission spectrum of BSA (a) with electronic absorption spectrum of  $[\text{Pd}(\text{bpy})(\text{acac})]\text{NO}_3$  (b). The concentrations of BSA and metal complex were equal to  $8 \mu\text{M}$ .

**Table 5**

The calculated energy transfer parameters in the Pd(II) complex-BSA system.

	$J(\text{cm}^3 \cdot \text{L} \cdot \text{mol}^{-1})$	E	r (nm)	$R_0$ (nm)
<b>Pd(II) complex-BSA system</b>	$1.085 \times 10^{-14}$	0.394	2.75	2.56

where  $F_0$  and  $F$  are the emission intensity of BSA without and with Pd(II) complex. Also,  $r_0$  and  $R_0$  are the binding distance and critical distance between donor and acceptor when the efficiency of transfer is 50%. The magnitude of  $R_0$  depends on the spectral attributes of the donor and acceptor and is obtained from the following Eq. (10):

$$R_0^6 = 8.8 \times 10^{-25} [K^2 N^{-4} \phi J(\lambda)] \quad (10)$$

where,  $N$  is the refractive index of a medium,  $\phi$  is the quantum yield of the donor without the acceptor and  $K^2$  is the spatial orientation factor of the dipole. The overlap integral of the donor fluorescence emission spectrum with the acceptor UV spectrum,  $J(\lambda)$ , was determined via Fig. 10 and numerical integration with the following Eq. (11):

$$J(\lambda) = \frac{\int_0^\infty F(\lambda) \varepsilon(\lambda) \lambda^4 d\lambda}{\int_0^\infty F(\lambda) d\lambda} \quad (11)$$

here,  $\varepsilon(\lambda)$  is the molar extinction coefficient of the acceptor at wavelength of  $\lambda$  and  $F(\lambda)$  is the corrected emission intensity of the donor. For Pd(II) complex-BSA system taking  $K^2 = 2/3$ ,  $N = 1.336$  and  $\phi = 0.15$  [77], the obtained values of  $J(\lambda)$ ,  $R_0$ ,  $r$  and  $E$  are listed in Table 5. The  $r$  value demonstrates that both acceptor ( $[\text{Pd}(\text{bpy})(\text{acac})]\text{NO}_3$ ) and donor (BSA) lie close together and can possess striking interaction with each other [78]. Moreover, the donor to acceptor distance ( $r < 8 \text{ nm}$ ) illustrates that the quenching mechanism in Pd(II) complex-BSA system is static [79,80] at high concentration, which supports the results obtained from fluorescence titration.

### 3.5.4. CT-DNA electrophoresis assay

The interaction ability of the Pd(II) complex with CT-DNA was studied via examining the effect of various concentrations of  $[\text{Pd}(\text{bpy})(\text{acac})]\text{NO}_3$  on CT-DNA, utilizing gel electrophoresis. Fluorescent dye EB that is inserted between nucleic acids bases (intercalation site) was utilized to visualize DNA in agarose gel. The DNA phosphate backbone is negatively charged and when located in an electric field, fragments of DNA move to the positively charged anode [81]. Since DNA has identical ratio of mass/charge, the DNA molecules can be distinguished according to their size. The CT-DNA electrophoretic mobility patterns in the absence and presence of diverse concentrations of  $[\text{Pd}(\text{bpy})(\text{acac})]\text{NO}_3$  are illustrated in

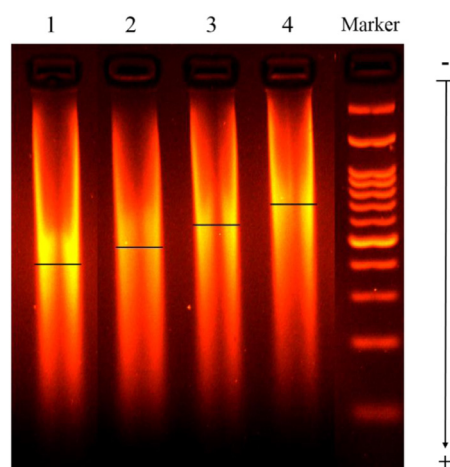


**Fig. 11.** Agarose gel electrophoresis pattern of: Marker (marker is circular DNA for checking the instrument), lane 1, untreated CT-DNA (4.23 mM) and lanes 2–4, 4.23 mM CT-DNA + (0.13, 0.20 and 0.26 mM) of  $[\text{Pd}(\text{bpy})(\text{acac})]\text{NO}_3$  complex.

Fig. 11. Free CT-DNA demonstrates a long band in lane 1. Lanes 2–4 obviously demonstrate that the complex induces mobility displacement of CT-DNA at different concentration without changing in the initial profile pattern. In the current work, no CT-DNA cleavage activity of  $[\text{Pd}(\text{bpy})(\text{acac})]\text{NO}_3$  has been observed. The retardation of CT-DNA band in the gel could be due to an increment in its mass or reduction of CT-DNA negative charge after interaction with Pd(II) complex.

### 3.5.5. Hydrodynamic measurement

Viscosity experiments were conducted to confirm the nature of binding mode of novel Pd(II) complex to CT-DNA. Viscosity measurements, a component of hydrodynamic methods, are sensitive to increase or decrease of DNA length and in the absence of spectroscopic and crystallographic data are regarded as the most efficient paths of probing the binding of small compounds and DNA [82]. A prevalent intercalative mode such as intercalation of ethidium bromide under proper conditions leads to a serious increment in the DNA viscosity because of an increment in the dissociation of base pairs at the intercalation positions and therefore an increasing in the length of the overall DNA. In groove binding (minor and major) or electrostatic mode, the DNA helix length is unchanged and leads to no apparent alteration in viscosity of DNA solution [83,84]. Besides, a non-classical and/or partial intercalation of molecule could screw (or bend) the DNA helix, decreasing its effectual length and viscosity [85,86]. The effects of increasing the synthesized Pd(II) complex and EB concentration on the CT-DNA viscosity are illustrated in Fig. 12. As can be observed in Fig. 12,

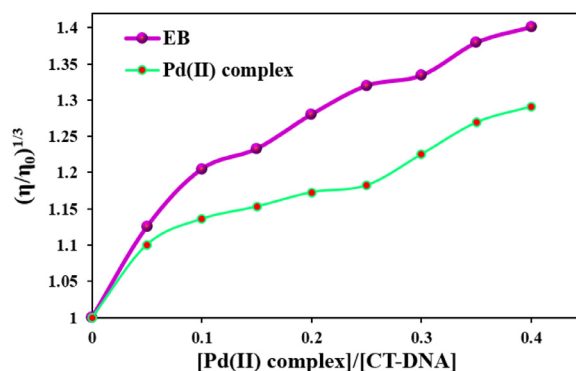


**Fig. 12.** The relative viscosities of CT-DNA with increasing concentration of Pd(II) complex at  $27 \pm 1^\circ \text{C}$ .  $[\text{CT-DNA}] = 60 \mu\text{M}$  and  $[\text{Pd(II) complex}] = [\text{EB}] = 0\text{--}24 \mu\text{M}$ .

with raising the value of  $r_1 = [\text{Pd(II) complex}]/[\text{CT-DNA}]$  (0 to 0.40), the relative viscosity of DNA solution increases significantly. This result may be due to the insertion of the aromatic rings (bpy and acac ligands) of  $[\text{Pd}(\text{bpy})(\text{acac})]\text{NO}_3$  into the CT-DNA base pairs resulting an increase in molecular length of CT-DNA at the intercalation site. As viscosity experiment result showed the mentioned complex binds with CT-DNA via intercalation mode, which is in agreement with the spectroscopic findings [87].

### 3.5.6. BSA-CD spectral

Circular Dichroism (CD), an intuitive spectroscopic technique to elucidate conformational changes of protein in protein-molecules interactions [88], was utilized in the current study. In Fig. 13(a), CD spectra of the free BSA and BSA with various concentrations of  $[\text{Pd}(\text{bpy})(\text{acac})]\text{NO}_3$  (0–65  $\mu\text{M}$ ) are shown. All CD spectra containing BSA and BSA-Pd(II) complex demonstrated two minima at around 208 and 222 nm, particular peaks for  $\alpha$ -helix structure that occur because of the  $\pi$ - $\pi^*$  and  $n$ - $\pi^*$  transitions in  $\alpha$ -helix. The intensity of peaks at the minima reflects the  $\alpha$ -helical amount of the protein. The related helical values of native BSA and interacted BSA were determined via the mean residual ellipticity values at 208 nm ( $MRE_{208}$ ) through the following relations (12) and (13) [89]:

$$[MRE]_{\lambda} = \frac{\text{Observed CD (deg.cm}^2\text{.dmol}^{-1})}{C_p n l \times 10} \quad (12)$$

$$\alpha\text{-Helix (\%)} = \frac{-MRE_{208} - 4000}{33000 - 4000} \times 100 \quad (13)$$

where  $C_p$ ,  $n$  and  $l$  represent BSA molar concentration, number of amino acid residues (583) and the cell path length, respectively. 4000 is related to the MRE of the random coil and  $\beta$ -form conformation at  $\lambda = 208$  nm while 33,000 is the magnitude of a pure  $\alpha$ -helix MRE at the same wavelength.

The calculated percentage values of  $\alpha$ -helix, parallel,  $\beta$ -turn, anti-parallel and random coil are summarized in Fig. 13(b). The results demonstrate an enhancement in negative ellipticity and  $\alpha$ -helix content from 72.6 to 79.7 and 83.4% at two concentrations (45 and 65  $\mu\text{M}$ ). All CD spectra were observed to be resembling in appearance shape without any notable move in the peak position (Fig. 13(a)), exhibiting stabilization of the secondary structure of BSA and interacted BSA with  $[\text{Pd}(\text{bpy})(\text{acac})]\text{NO}_3$ . It also suggests that the BSA structure was mainly  $\alpha$ -helix even after interaction with the complex. Here, it is interesting to look at the coincidence of CD results with that of UV-Vis discussed in Section 3.5.1. We saw in Section 3.5.1 that when BSA comes in contact with increasing amounts of Pd(II) complex, its absorption decreases at 280 nm. This decrease is due to the hiding of the absorbing BSA groups from UV light and the contraction of the native BSA happens. In

CD studies, the decrease in percentage of  $\beta$ -turn and random coil with  $\alpha$ -helix rise can be attributed to the occurrence of a kind of contraction in the native structure of BSA. Thus, the CD and UV-Vis studies display the same conformational alterations in the BSA structure and endorse each other.

### 3.5.7. Docking on macromolecules

*In-silico* molecular docking, which identifies the binding sites of small molecules on macromolecules, was also utilized to gain unique insights into the interaction of Pd(II) complex with DNA and BSA. The optimized structure of the complex was docked into the DNA and BSA fragments. The best pose of the complex with DNA (with more negative  $\Delta G^\circ$ ), is demonstrated in Fig. 14. This figure demonstrates the nucleotides and the complex structures involved in the interactions along with the distance between them. It is evident from this figure that the entire docked complex is located within the intercalation site of DNA between cytosine and guanine on both strands, leads to the existence of hydrophobic interactions. In the other word, there are  $\pi$ -alkyl interactions between acac ligand of Pd(II) complex and Cyt4 and Gua5 of DNA. The  $\pi$ - $\pi$  interactions are also found between the planar rings of bpy ligand and Gua5 and Cyt4 of DNA strand.  $\Delta G^\circ$  of the complex with DNA was evaluated to be  $-7.22$  kcal.  $\text{mol}^{-1}$ , which is consistent with the UV-Vis result ( $\Delta G^\circ_{\text{UV-Vis}} = -7.37$  kcal.  $\text{mol}^{-1}$ ). Therefore, taking into account the findings of the docking simulation and the experimental procedures, it could be concluded that the Pd(II) complex binds to DNA by intercalation.

Two potential interaction sites on BSA (site I and II) were investigated in the case of the BSA-docking simulation (Fig. 15). The obtained  $\Delta G^\circ$  of the complex to BSA site I ( $\Delta G^\circ = -6.19$  kcal.  $\text{mol}^{-1}$ ) was more negative than that of site II ( $\Delta G^\circ = -5.58$  kcal.  $\text{mol}^{-1}$ ), suggesting the complex primarily is located in BSA site I. So, for further analysis of docking result, we concentrate on BSA site I findings. The obtained  $\Delta G^\circ_{\text{UV-Vis}}$  ( $-4.45$  kcal/mol) for BSA interaction, varies marginally from the computational value, due to the fact that the experimental method was conducted in solution environment (body physiological condition) while the docking simulation results has been obtained in the gas phase and the effect of water and working buffer have been neglected [90]. The values of vdW+Hbond+desolve and electrostatic energies were evaluated to be  $-6.19$  and  $0.00$  kcal.  $\text{mol}^{-1}$ , respectively, demonstrating that hydrogen bond and van der Waals forces play a vital function, while electrostatic attraction has no particular role in the interaction process. Docking simulation illustrated that the newly complex interacts with the following BSA residues: Glu100, Leu103, Ser104, Lys106, Tyr147, Ile202, Gln203, Lys242, Cys245 and His246. A hydrogen bond is observed between His246 and the oxygen atom of the Pd(II) complex with the distance of 3.1 Å. Other residues are involved in the formation of van der Waals force between the BSA

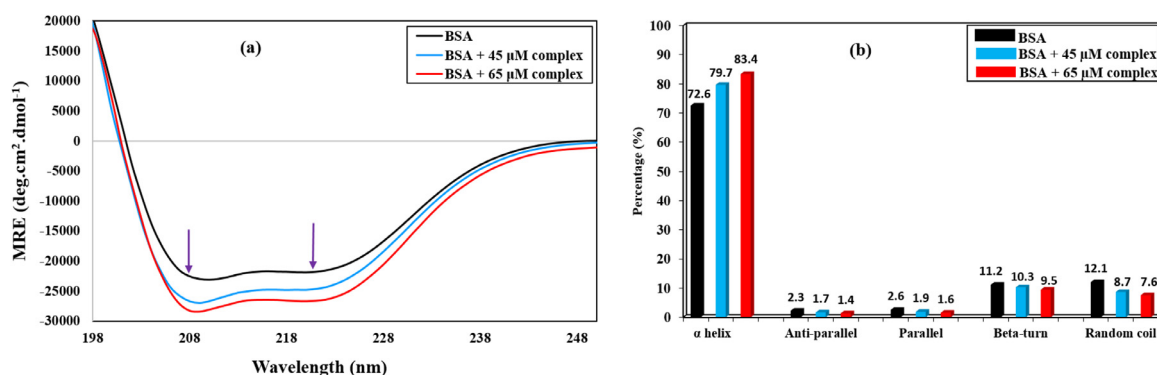


Fig. 13. (a) Circular dichroism spectra of native BSA (5.5  $\mu\text{M}$ ) with increasing concentration of  $[\text{Pd}(\text{bpy})(\text{acac})]\text{NO}_3$  complex (0–65  $\mu\text{M}$ ). (b) the values and relative percentages of secondary structure elements of BSA in the absence (black column) and presence (blue and red column) of  $[\text{Pd}(\text{bpy})(\text{acac})]\text{NO}_3$  complex.

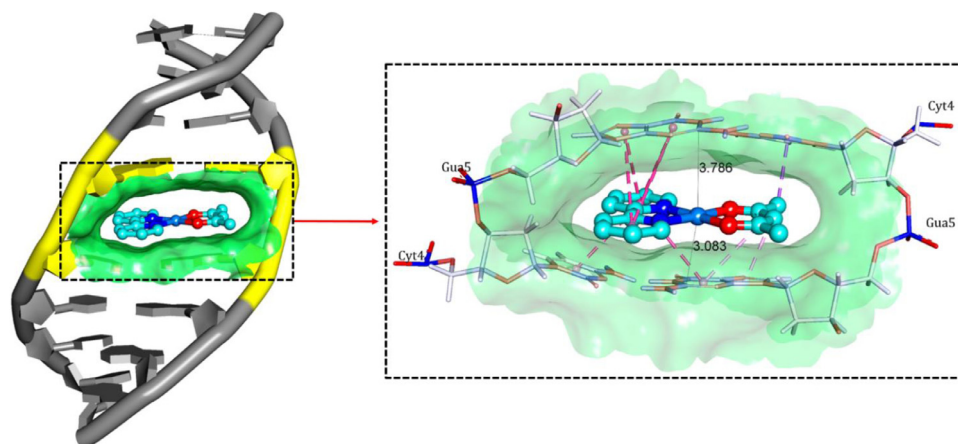


Fig. 14. Docking pose of Pd(II) complex with DNA.

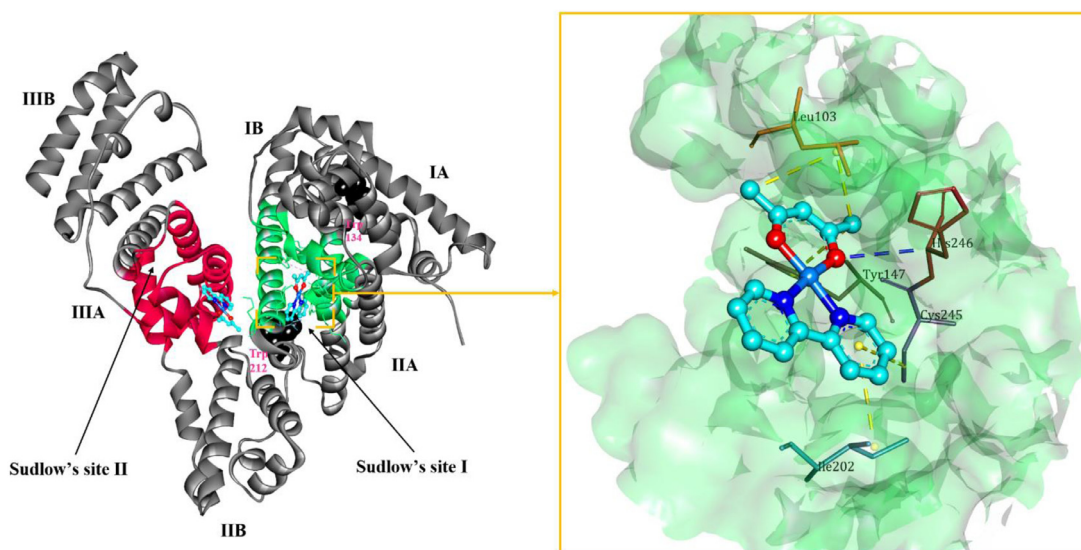


Fig. 15. Docking pose of Pd(II) complex with BSA.

and the complex. The distance between CH<sub>3</sub> group of acac ligand in [Pd(bpy)(acac)]NO<sub>3</sub> and the O atom in C = O group of Trp134 residue is 21.60 Å (2.16 nm) evidently lower than 8 nm, which is absolutely in line with the result of the FRET calculation. The obtained results from computational ( $\Delta G^{\circ}_{\text{DNA, docking}} = -7.22$  and  $\Delta G^{\circ}_{\text{BSA, docking}} = -6.19$  kcal. mol<sup>-1</sup>) and experimental approaches imply the well binding affinities of the complex with CT-DNA via intercalation site and moderate interaction with BSA via van der Waals forces and hydrogen bonding.

#### 4. Conclusion

Novel mononuclear Pd(II) complex with cytotoxicity activity much better than cisplatin was synthesized and fully characterized via various physicochemical techniques. The findings of spectroscopic methods along with DFT calculation indicated that the PdN<sub>2</sub>O<sub>2</sub> lies in the aromatic plane of 2,2'-bipyridine which may improve its binding behavior. The lipophilicity determination of the new complex was performed in terms of log P and the obtained value was higher than that of cisplatin. *In-vitro* biomolecules interaction profiles of the complex utilizing in-detail fluorescence and UV-Vis methods supported the fact that it binds to CT-DNA by intercalation mode and demonstrates a weaker binding affinity to BSA. UV-Vis as well as CD studies displayed the same conformational alterations in the native structure of the BSA and are mu-

tually supporting. In addition, DNA-viscosity measurements, DNA-gel electrophoresis assay, BSA-FRET calculation provided more insights into the interaction mechanisms of the complex with DNA and BSA. MEP map revealed the electrophilic and nucleophilic centers of the complex. FMO analysis showed the charge transfer occurs from acac to bpy ligand within the complex. *In-silico* molecular docking results exhibited an excellent agreement with the experimental finding in the case of binding mechanism and energy of the synthesized compound with macromolecules. Thus, the structural variation of N–N and O–O donor set of palladium(II) complex towards nucleic acid and albumin provide us more detail about the binding affinities of drug-macromolecules and are of vital relevance in biochemistry and pharmacy.

#### Credit author statement

Mehran Feizi-Dehnayebi: Ph.D. student,  
Effat Dehghanian: Guide,  
Hassan Mansouri-Torshizi: Co-Guide.

#### Declaration of Competing Interest

The authors declare that they have no known competing financial interests or personal relationships that could have appeared to influence the work reported in this paper.

## Acknowledgements

The authors gratefully acknowledge the University of Sistan and Baluchestan for the essential supporting of this research.

## Supplementary materials

Supplementary material associated with this article can be found, in the online version, at doi:10.1016/j.molstruc.2021.130535.

## References

- [1] B. Rosenberg, L. Vancamp, J.E. Trosko, V.H. Mansour, Platinum compounds: a new class of potent antitumor agents, *Nature* 222 (1969) 385–386.
- [2] Y. Kasherian, S. Sturup, D. Gibson, Is glutathione the major cellular target of cisplatin? A study of the interactions of cisplatin with cancer cell extracts, *J. Med. Chem.* 52 (2009) 4319–4328.
- [3] J.A. Garcia, R. Dreicer, Systemic chemotherapy for advanced bladder cancer: update and controversies, *J. Clin. Oncol.* 24 (2006) 5545–5551.
- [4] K.J. Barnham, M.I. Djuran, P.D.S. Murdoch, J.D. Ranford, P.J. Sadler, Ring-opened adducts of the anticancer drug carboplatin with sulfur amino acids, *Inorg. Chem.* 35 (1996) 1065–1072.
- [5] F. Huq, H. Tayyem, P. Beale, J.Q. Yu, Studies on the activity of three palladium (II) compounds of the form: trans-PdL<sub>2</sub>Cl<sub>2</sub> where L= 2-hydroxypyridine, 3-hydroxypyridine, and 4-hydroxypyridine, *J. Inorg. Biochem.* 101 (2007) 30–35.
- [6] W. Friebolin, G. Schilling, M. Zöller, E. Amtmann, Antitumoral activity of non-platinum xanthate complexes, *J. Med. Chem.* 48 (2005) 7925–7931.
- [7] A.R. Kapdi, I.J. Fairlamb, Anti-cancer palladium complexes: a focus on PdX<sub>2</sub>L<sub>2</sub>, palladacycles and related complexes, *Chem. Soc. Rev.* 43 (2014) 4751–4777.
- [8] F. Blau, Über die trockene Destillation von pyridincarbon-säuren Salzen, *Monatsh. für Chemie und verwandte Teile anderer Wissenschaften* 10 (1889) 375–388.
- [9] J.F. Steinbach, H. Freiser, Acetylacetone, *Anal. Chem.* 25 (1953) 881–884.
- [10] M. Aleksić, V. Kapetanović, An overview of the optical and electrochemical methods for detection of DNA-drug interactions, *Acta Chim. Slov.* 61 (2014) 555–573.
- [11] D.C. Carter, B. Chang, J.X. Ho, K. Keeling, Z. Krishnasami, Preliminary crystallographic studies of four crystal forms of serum albumin, *Eur. J. Biochem.* 226 (1994) 1049–1052.
- [12] T. Peters Jr., Serum albumin, in: *Advances in Protein Chemistry*, Elsevier, 1985, pp. 161–245.
- [13] S. Shahraki, F. Shiri, H. Mansouri-Torshizi, J. Shahraki, Characterization of the interaction between a platinum (II) complex and human serum albumin: spectroscopic analysis and molecular docking, *J. Iran. Chem. Soc.* 13 (2016) 723–731.
- [14] A.D. Becke, Density-functional exchange-energy approximation with correct asymptotic behavior, *Phys. Rev. A* 38 (1988) 3098.
- [15] C. Lee, W. Yang, R.G. Parr, Development of the Colle-Salvetti correlation-energy formula into a functional of the electron density, *Phys. Rev. B* 37 (1988) 785.
- [16] R.G. Mohamed, F.M. Elantabli, A.A.A. Aziz, H. Moustafa, S.M. El-Medani, Synthesis, characterization, NLO properties, antimicrobial, CT-DNA binding and DFT modeling of Ni (II), Pd (II), Pt (II), Mo (IV) and Ru (I) complexes with NOS Schiff base, *J. Mol. Struct.* 1176 (2019) 501–514.
- [17] K.A. Peterson, D. Figgen, M. Dolg, H. Stoll, Energy-consistent relativistic pseudopotentials and correlation consistent basis sets for the 4 d elements Y–Pd, *J. Chem. Phys.* 126 (2007) 124101.
- [18] D. Feller, The role of databases in support of computational chemistry calculations, *J. Comput. Chem.* 17 (1996) 1571–1586.
- [19] K.L. Schuchardt, B.T. Didier, T. Elsethagen, L. Sun, V. Gurumoorthi, J. Chase, J. Li, T.L. Windus, Basis set exchange: a community database for computational sciences, *J. Chem. Inf. Model.* 47 (2007) 1045–1052.
- [20] S. Jagadeesan, V. Balasubramanian, P. Baumann, M. Neuburger, D. Häussinger, C.G. Palivan, Water-soluble Co (III) complexes of substituted phenanthrolines with cell selective anticancer activity, *Inorg. Chem.* 52 (2013) 12535–12544.
- [21] A. Divsalar, A. Saboury, R. Yousefi, A. Moosavi-Movahedi, H. Mansoori-Torshizi, Spectroscopic and cytotoxic studies of the novel designed palladium (II) complexes:  $\beta$ -Lactoglobulin and K562 as the targets, *Int. J. Biol. Macromol.* 40 (2007) 381–386.
- [22] S. Sarkar, P. Bhattacharjee, K. Bhadra, DNA binding and apoptotic induction ability of harmalol in HepG2: biophysical and biochemical approaches, *Chem. Biol. Interact.* 258 (2016) 142–152.
- [23] A. Zianna, G.D. Geromichalos, A. Pekou, A.G. Hatzidimitriou, E. Coutouli-Argyropoulou, M. Lalia-Kantouri, A.A. Pantazaki, G. Psomas, A palladium (II) complex with the Schiff base 4-chloro-2-(N-ethyliminomethyl)-phenol: synthesis, structural characterization, and in vitro and in silico biological activity studies, *J. Inorg. Biochem.* 199 (2019) 110792.
- [24] A. Maity, U. Pal, B. Chakraborty, C. Sengupta, A. Sau, S. Chakraborty, S. Basu, Preferential photochemical interaction of Ru (III) doped carbon nano dots with bovine serum albumin over human serum albumin, *Int. J. Biol. Macromol.* 137 (2019) 483–494.
- [25] M.A. Teir, J. GHITHAN, S. DARWISH, M.M. ABU-HADID, Multi-spectroscopic investigation of the interactions between cholesterol and human serum albumin, *J. Appl. Biol. Sci.* 6 (2012) 45–55.
- [26] M. Feizi-Dehnyabi, E. Dehghanian, H. Mansouri-Torshizi, A novel palladium (II) antitumor agent: synthesis, characterization, DFT perspective, CT-DNA and BSA interaction studies via in-vitro and in-silico approaches, *Spectrochim. Acta Part A* 249 (2021) 119215.
- [27] J.R. Lakowicz, Plasmonics in biology and plasmon-controlled fluorescence, *Plasmonics* 1 (2006) 5–33.
- [28] Y.-c. Liu, Z.-y. Yang, Synthesis, crystal structure, antioxidation and DNA binding properties of binuclear Ho (III) complexes of Schiff-base ligands derived from 8-hydroxyquinoline-2-carboxaldehyde and four aroylhydrazines, *J. Organomet. Chem.* 694 (2009) 3091–3101.
- [29] G. Zhang, Y. Ma, L. Wang, Y. Zhang, J. Zhou, Multispectroscopic studies on the interaction of maltol, a food additive, with bovine serum albumin, *Food Chem.* 133 (2012) 264–270.
- [30] J.R. Lakowicz, G. Weber, Quenching of fluorescence by oxygen. Probe for structural fluctuations in macromolecules, *Biochemistry* 12 (1973) 4161–4170.
- [31] S. Shahraki, M.H. Majd, A. Heydari, Novel tetradentate Schiff base zinc (II) complex as a potential antioxidant and cancer chemotherapeutic agent: insights from the photophysical and computational approach, *J. Mol. Struct.* 1177 (2019) 536–544.
- [32] S. Shahraki, F. Shiri, M.H. Majd, Z. Razmara, Comparative study on the anti-cancer activities and binding properties of a hetero metal binuclear complex [Co (dipic) 2Ni (OH)<sub>2</sub> 5]• 2H<sub>2</sub>O (dipic= dipicolinate) with two carrier proteins, *J. Pharm. Biomed. Anal.* 145 (2017) 273–282.
- [33] A. Heydari, H. Mansouri-Torshizi, Design, synthesis, characterization, cytotoxicity, molecular docking and analysis of binding interactions of novel acetylacetonatopalladium (II) alanine and valine complexes with CT-DNA and BSA, *RSC Adv.* 6 (2016) 96121–96137.
- [34] K. Liu, G. Chang, H. Yan, Z. Li, M. Hong, M. Niu, Dimethyltin (IV) complexes derived from hydroxamic acid and acylhydrazone ligands: synthesis, DNA/bovine serum albumin interaction and cytotoxicity, *Appl. Organomet. Chem.* 32 (2018) e3973.
- [35] J. Yang, C. Wu, H. Martinez, Direct determination of absolute circular dichroism data and calibration of commercial instrument, *Anal. Chem.* 53 (1981) 778–782.
- [36] P. Manavalan, W.C. Johnson Jr, Variable selection method improves the prediction of protein secondary structure from circular dichroism spectra, *Anal. Biochem.* 167 (1987) 76–85.
- [37] G.M. Morris, M. Lim-Wilby, Molecular docking, in: *Molecular Modeling of Proteins*, Springer, 2008, pp. 365–382.
- [38] G.M. Morris, D.S. Goodsell, R.S. Halliday, R. Huey, W.E. Hart, R.K. Belew, A.J. Olson, Automated docking using a Lamarckian genetic algorithm and an empirical binding free energy function, *J. Comput. Chem.* 19 (1998) 1639–1662.
- [39] G.M. Morris, R. Huey, A.J. Olson, Using autodock for ligand-receptor docking, *Curr. Protoc. Bioinform.* 24 (2008) 8.14. 11–18.14. 40.
- [40] R.J. Angelici, R.J. Angelici, *Synthesis and Technique in Inorganic Chemistry*, Saunders Philadelphia, 1969.
- [41] K. Nakamoto, *Infrared and Raman Spectra of Inorganic and Coordination Compounds*, John Wiley and Sons, Inc., New York, 1986.
- [42] P. Bladon, in: *Spectroscopic Identification of Organic Compounds*, By RM Silverstein and GC Bassler, John Wiley and Sons Inc., New York and Chichester, Sussex, 1967, p. 256. + x.£ 5.3. Od \$10.95, students edition£ 3.0. 0, *Organic Magnetic Resonance*, 1 (1969) 277–277.
- [43] K. Nakamoto, *Infrared and Raman Spectra of Inorganic and Coordination Compounds* (Part A: Theory and Applications in Inorganic Chemistry)(Volume 1A)(Part B: Applications in Coordination, Organometallic, and Bioinorganic Chemistry)(Volume 1B), John Wiley & Sons, NY, 1997 Incorporated.
- [44] X.-Q. Song, Y.-W. Wang, J.-R. Zheng, W.-S. Liu, M.-Y. Tan, Synthesis and spectroscopic properties of lanthanide nitrate complexes with a new amide-based quinoxaline-2, 3-dione ligand, *Spectrochim. Acta Part A* 68 (2007) 701–704.
- [45] O. Kozachkova, N. Tsaryk, V. Pekhnyo, V. Trachevskiy, A. Rozhenko, V. Dyakonko, Complexation of dichloro (ethylenediamine) palladium (II) with 1-hydroxyethylidene-1, 1-diphosphonic acid, *Inorganica Chim. Acta* 474 (2018) 96–103.
- [46] J. Forniés, F. Martínez, R. Navarro, E.P. Urriolabeitia, Synthesis and reactivity of acetylacetonato- $\text{C}_\gamma$  complexes of M(II) (M Pd or Pt): x-ray crystal structure of [Pd (C<sub>6</sub>F<sub>5</sub>)(OOCPh)(bipy)]•CHCl<sub>3</sub>, *J. Organomet. Chem.* 495 (1995) 185–194.
- [47] E. Scrocco, J. Tomasi, The electrostatic molecular potential as a tool for the interpretation of molecular properties, in: *New Concepts II*, Springer, 1973, pp. 95–170.
- [48] T. Koopmans, Über die Zuordnung von Wellenfunktionen und Eigenwerten zu den einzelnen Elektronen eines Atoms, *Physica* 1 (1934) 104–113.
- [49] R.G. Parr, L.v. Szentpaly, S. Liu, Electrophilicity index, *J. Am. Chem. Soc.* 121 (1999) 1922–1924.
- [50] R.G. Parr, R.G. Pearson, Absolute hardness: companion parameter to absolute electronegativity, *J. Am. Chem. Soc.* 105 (1983) 7512–7516.
- [51] S. Shahraki, A. Heydari, New zinc (II) N<sub>4</sub> tetradentate Schiff base complex: a potential cytotoxic metallodrug and simple precursor for the preparation of ZnO nanoparticles, *Colloids Surf. B* 160 (2017) 564–571.
- [52] E.E. Meyer, K.J. Rosenberg, J. Israelachvili, Recent progress in understanding hydrophobic interactions, *Proc. Natl. Acad. Sci.* 103 (2006) 15739–15746.
- [53] V.T. Yilmaz, C. Işcel, O.R. Turgut, M. Aygun, M. Erkiş, M.H. Turkmendir, E. Ulukaya, Synthesis, structures and anticancer potentials of platinum (II) saccharinate complexes of tertiary phosphines with phenyl and cyclohexyl groups targeting mitochondria and DNA, *Eur. J. Med. Chem.* 155 (2018) 609–622.

- [54] A.K. Ghose, V.N. Viswanadhan, J.J. Wendoloski, A knowledge-based approach in designing combinatorial or medicinal chemistry libraries for drug discovery. 1. A qualitative and quantitative characterization of known drug databases, *J. Comb. Chem.* 1 (1999) 55–68.
- [55] A. Divsalar, M. Razmi, A.A. Saboury, H. Mansouri-Torshizi, F. Ahmad, Biological evaluation of a new synthesized Pt (II) complex by cytotoxic and spectroscopic studies, *Cell Biochem. Biophys.* 71 (2015) 1415–1424.
- [56] R. Arif, M. Rana, S. Yasmeen, M.S. Khan, M. Abid, M. Khan, Facile synthesis of chalcone derivatives as antibacterial agents: synthesis, DNA binding, molecular docking, DFT and antioxidant studies, *J. Mol. Struct.* 1208 (2020) 127905.
- [57] F. Xue, C.-Z. Xie, Y.-W. Zhang, Z. Qiao, X. Qiao, J.-Y. Xu, S.-P. Yan, Two new dicopper (II) complexes with oxamido-bridged ligand: synthesis, crystal structures, DNA binding/cleavage and BSA binding activity, *J. Inorg. Biochem.* 115 (2012) 78–86.
- [58] P. Sathyadevi, P. Krishnamoorthy, N.S. Bhuvanesh, P. Kalaiselvi, V.V. Padma, N. Dharmaraj, Organometallic ruthenium (II) complexes: synthesis, structure and influence of substitution at azomethine carbon towards DNA/BSA binding, radical scavenging and cytotoxicity, *Eur. J. Med. Chem.* 55 (2012) 420–431.
- [59] X.-W. Li, X.-H. Zhao, Y.-T. Li, Z.-Y. Wu, Synthesis and crystal structure of bi-copper (II) complexes: the influence of bridging ligands on DNA/BSA binding behaviors and in vitro antitumor activity, *Inorganica Chim. Acta* 488 (2019) 219–228.
- [60] S.Y. Ebrahimipour, I. Sheikhshoae, M. Mohamadi, S. Suarez, R. Baggio, M. Khaleghi, M. Torkzadeh-Mahani, A. Mostafavi, Synthesis, characterization, X-ray crystal structure, DFT calculation, DNA binding, and antimicrobial assays of two new mixed-ligand copper (II) complexes, *Spectrochim. Acta Part A* 142 (2015) 410–422.
- [61] S.Y. Ebrahimipour, M. Mohamadi, M.T. Mahani, J. Simpson, J.T. Mague, I. Sheikhshoae, Synthesis and structure elucidation of novel salophen-based dioxo-uranium (VI) complexes: in-vitro and in-silico studies of their DNA/BSA-binding properties and anticancer activity, *Eur. J. Med. Chem.* 140 (2017) 172–186.
- [62] K. Karami, M. Alinaghi, Z. Amirghofran, J. Lipkowski, A.A. Momtazi-borojeni, A saccharinate-bridged palladacyclic dimer with a Pd–Pd bond: experimental and molecular docking studies of the interaction with DNA and BSA and in vitro cytotoxicity against human cancer cell lines, *New J. Chem.* 42 (2018) 574–586.
- [63] S. Shahraki, F. Shiri, H. Beyzaei, F. Khosravi, Synthesis, characterization, protein interaction and antibacterial activity of a lanthanum (iii) complex [La (Trp) 3 (OH 2) 2](Trp= tryptophan) as a new precursor for synthesis of La 2 O 2 CO 3 nanoparticles, *New J. Chem.* 41 (2017) 8413–8421.
- [64] X. Li, Q. Wang, Y. Qing, Y. Lin, Y. Zhang, X. Qian, J. Cui, Novel DNA intercalators without basic side chains as efficient antitumor agents: design, synthesis and evaluation of benzo-[c, d]-indol-malononitrile derivatives, *Bioorg. Med. Chem.* 18 (2010) 3279–3284.
- [65] M. Mohamadi, A. Hassankhani, S.Y. Ebrahimipour, M. Torkzadeh-Mahani, In vitro and in silico studies of the interaction of three tetrazoloquinazoline derivatives with DNA and BSA and their cytotoxicity activities against MCF-7, HT-29 and DPSC cell lines, *Int. J. Biol. Macromol.* 94 (2017) 85–95.
- [66] G. Psomas, Mononuclear metal complexes with ciprofloxacin: synthesis, characterization and DNA-binding properties, *J. Inorg. Biochem.* 102 (2008) 1798–1811.
- [67] I. Yousuf, M. Bashir, F. Arjmand, S. Tabassum, Multispectroscopic insight, morphological analysis and molecular docking studies of Cull-based chemotherapeutic drug entity with human serum albumin (HSA) and bovine serum albumin (BSA), *J. Biomol. Struct. Dyn.* 37 (2019) 3290–3304.
- [68] M. Dustkami, H. Mansouri-Torshizi, Refolding and unfolding of CT-DNA by newly designed Pd (II) complexes. Their synthesis, characterization and anti-tumor effects, *Int. J. Biol. Macromol.* 99 (2017) 319–334.
- [69] Z. Moradi, M. Khorasani-Motlagh, A.R. Rezvani, M. Noroozifar, Electronic and fluorescent studies on the interaction of DNA and BSA with a new ternary praseodymium complex containing 2, 9-dimethyl 1, 10-phenanthroline and antibacterial activities testing, *J. Biomol. Struct. Dyn.* 37 (2019) 2283–2295.
- [70] M. Saeidifar, R. Sabbaghzadeh, N.A. Nasab, Biophysical investigation and antitumor potential of heterocyclic palladium-based agent: cytotoxicity, spectroscopic and molecular docking approaches in interaction with human serum albumin, *Polycycl. Aromat. Compd.* (2020) 1–19.
- [71] K.L. Zhou, D.Q. Pan, Y.Y. Lou, J.H. Shi, Intermolecular interaction of fosinopril with bovine serum albumin (BSA): the multi-spectroscopic and computational investigation, *J. Mol. Recognit.* 31 (2018) e2716.
- [72] L. Yang, D. Huo, C. Hou, M. Yang, H. Fa, X. Luo, Interaction of monosulfonate tetraphenyl porphyrin (H2TPPS1) with plant-esterase: determination of the binding mechanism by spectroscopic methods, *Spectrochim. Acta Part A* 78 (2011) 1349–1355.
- [73] Z. Yang, R. Tang, Z. Zhang, Synthesis and luminescent properties of Tb (III) complex with a novel pyrazolone ligand and its interaction with bovine serum albumin, *J. Mol. Struct.* 1030 (2012) 19–25.
- [74] S. Shahraki, F. Shiri, M. Saeidifar, Evaluation of in silico ADMET analysis and human serum albumin interactions of a new lanthanum (III) complex by spectroscopic and molecular modeling studies, *Inorganica Chim. Acta* 463 (2017) 80–87.
- [75] J. Lakowicz, Energy transfer. Ch. 13, Principles of Fluorescence Spectroscopy, Kluwer Academic/Plenum Publishers, New York, 1999.
- [76] L. Sheng, H. Ding, Z. Wang, C. Song, Binding of amphiphilic p (DMAEMA79-b-AZOM5) diblock copolymer with bovine serum albumin—a spectroscopic investigation with warfarin and ibuprofen as site markers, *J. Mol. Struct.* 979 (2010) 152–159.
- [77] L. Cyril, J. Earl, W. Sperry, in: *Biochemists Handbook*, E & FN Epon Led, Press, London, 1961, p. 83.
- [78] C.-Q. Jiang, M.-X. Gao, X.-Z. Meng, Study of the interaction between daunorubicin and human serum albumin, and the determination of daunorubicin in blood serum samples, *Spectrochim. Acta Part A* 59 (2003) 1605–1610.
- [79] M. Mathew, S. Sreedhanya, P. Manoj, C. Aravindakumar, U.K. Aravind, Exploring the interaction of bisphenol-S with serum albumins: a better or worse alternative for bisphenol A? *J. Phys. Chem. B* 118 (2014) 3832–3843.
- [80] S. Shahraki, F. Shiri, M. Saeidifar, Synthesis, characterization, in silico ADMET prediction, and protein binding analysis of a novel zinc (II) Schiff-base complex: application of multi-spectroscopic and computational techniques, *J. Biomol. Struct. Dyn.* 36 (2018) 1666–1680.
- [81] J.-H. He, D.-R. Xiao, H.-Y. Chen, D.-Z. Sun, S.-W. Yan, X. Wang, Z.-L. Ye, Q.-L. Luo, E.-B. Wang, A series of 2D metal–quinolone complexes: syntheses, structures, and physical properties, *J. Solid State Chem.* 198 (2013) 279–288.
- [82] L.H. Abdel-Rahman, A.M. Abu-Dief, H. Moustafa, S.K. Hamdan, Ni (II) and Cu (II) complexes with ONNO asymmetric tetradentate Schiff base ligand: synthesis, spectroscopic characterization, theoretical calculations, DNA interaction and antimicrobial studies, *Appl. Organomet. Chem.* 31 (2017) e3555.
- [83] D.S. Raja, N.S. Bhuvanesh, K. Natarajan, Structure–activity relationship study of copper (II) complexes with 2-oxo-1, 2-dihydroquinoline-3-carbaldehyde (4'-methylbenzoyl) hydrazone: synthesis, structures, DNA and protein interaction studies, antioxidative and cytotoxic activity, *JBIC J. Biol. Inorg. Chem.* 17 (2012) 223–237.
- [84] L.H. Abdel-Rahman, A.M. Abu-Dief, E.F. Newair, S.K. Hamdan, Some new nano-sized Cr (III), Fe (II), Co (II), and Ni (II) complexes incorporating 2-((E)-(pyridine-2-ylimino) methyl) naphthalen-1-ol ligand: structural characterization, electrochemical, antioxidant, antimicrobial, antiviral assessment and DNA interaction, *J. Photochem. Photobiol. B* 160 (2016) 18–31.
- [85] Y.Y. Lü, L.H. Gao, M.J. Han, K.Z. Wang, Synthesis and the effect of a peripheral N-arylcarbazole moiety on the acid-base and DNA binding properties of a novel ruii complex, *Eur. J. Inorg. Chem.* 2006 (2006) 430–436.
- [86] S. Satyanarayana, J.C. Dabrowiak, J.B. Chaires, Tris (phenanthroline) ruthenium (II) enantiomer interactions with DNA: mode and specificity of binding, *Biochemistry* 32 (1993) 2573–2584.
- [87] N. Ganji, A. Rambabu, N. Vamsikrishna, S. Daravath, Copper (II) complexes with isoxazole Schiff bases: synthesis, spectroscopic investigation, DNA binding and nuclease activities, antioxidant and antimicrobial studies, *J. Mol. Struct.* 1173 (2018) 173–182.
- [88] X. Cao, Z. Yang, Y. He, Y. Xia, Y. He, J. Liu, Multispectroscopic exploration and molecular docking analysis on interaction of eriocitrin with bovine serum albumin, *J. Mol. Recognit.* 32 (2019) e2779.
- [89] Y.-H. Chen, J.T. Yang, K.H. Chau, Determination of the helix and  $\beta$  form of proteins in aqueous solution by circular dichroism, *Biochemistry* 13 (1974) 3350–3359.
- [90] M. Shaghghi, S. Rashtbari, S. Vejdani, G. Dehghan, A. Jouyban, R. Yekta, Exploring the interactions of a Tb (III)-quercetin complex with serum albumins (HSA and BSA): spectroscopic and molecular docking studies, *Luminescence* 35 (2020) 512–524.